Journal of Colloid and Interface Science 674 (2024) 209–224

Contents lists available at ScienceDirect

Journal of Colloid And Interface Science

journal homepage: www.elsevier.com/locate/jcis

Regular Article

Temperature response of sucrose palmitate solutions: Role of ratio between monoesters and diesters

N. Pagureva [a,1], D. Cholakova [a,1], Z. Mitrinova [a], M. Hristova [a], N. Burdzhiev [b], S. Tcholakova [a,*]

[a] Department of Chemical and Pharmaceutical Engineering, Faculty of Chemistry and Pharmacy, Sofia University, 1164 Sofia, Bulgaria
[b] Department of Organic Chemistry and Pharmacognosy, Faculty of Chemistry and Pharmacy, Sofia University, 1164 Sofia, Bulgaria

GRAPHICAL ABSTRACT

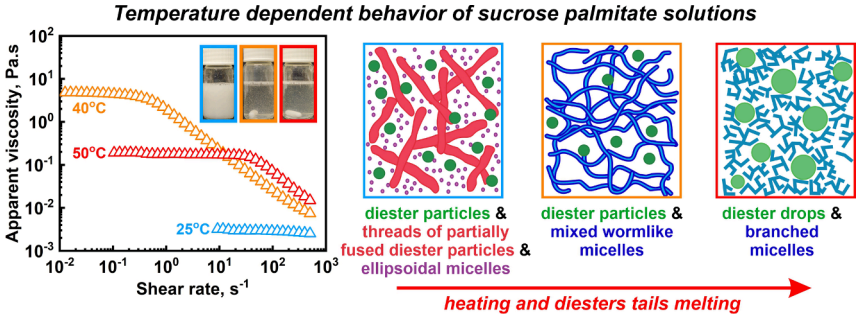

ARTICLE INFO

Keywords:
Micelles
Particles
Rheology
Aggregation
Heating/cooling
Biodegradable surfactant

ABSTRACT

Hypothesis: Aqueous solutions of long-chain water-soluble sucrose ester surfactants exhibit non-trivial response to temperature variations, revealing a peak in viscosity around 40–50 °C. While previous investigations have explored the structures within sucrose stearate systems at various constant temperatures, a comprehensive understanding of the entire temperature dependence and the underlying molecular factors, contributing to this phenomenon is currently missing.

Experiments: Temperature dependent properties and supramolecular structures formed in aqueous solutions of commercial sucrose palmitate were examined using SAXS/WAXS, DSC, optical microscopy, rheological measurements, NMR, and cryo-TEM.

Findings: The underlying mechanism governing this unusual behavior is revealed and is shown to relate to the mono- to di-esters ratio in the solutions. Solutions primarily containing sucrose monoesters (monoesters molecules ≳ 98% of all surfactant molecules) exhibit behavior typical of nonionic surfactants, with minimal changes with temperature. In contrast, the coexistence of mono- and di-esters results in the formation of discrete monodisperse diester particles and a network of partially fused diester particles at low temperature. As the temperature approaches the diesters' melting point, wormlike mixed micelles form, causing a viscosity peak. The height of this peak increases significantly with the diester concentration. Further temperature increase leads to

* Corresponding author at: Department of Chemical and Pharmaceutical Engineering, Faculty of Chemistry and Pharmacy, Sofia University, 1 James Bourchier Ave., 1164 Sofia, Bulgaria.
E-mail address: sc@lcpe.uni-sofia.bg (S. Tcholakova).
[1] These authors contributed equally to this paper.

https://doi.org/10.1016/j.jcis.2024.06.061
Received 20 March 2024; Received in revised form 3 June 2024; Accepted 6 June 2024
Available online 21 June 2024

fluidization of surfactant tails and formation of branched micelles, while excess diester molecules phase separate into distinct droplets.

1. Introduction

The growing recognition of the potential harmful effects of synthetic surfactants on the environment and human health has sparked a significantly increased interest in the development of natural surfactants. Currently, one of the primary groups of plant-derived surfactants under investigation is based on sucrose and fatty acids [1,2]. Among these, two main classes stand out – alkyl polyglycosides (APGs) and sucrose esters (SEs). Both types of surfactants consist of a carbohydrate hydrophilic head and an alkyl fatty acid residue as the hydrophobic tail. However, while APGs typically have several polymerized saccharide units in their hydrophilic head and a single hydrophobic acyl chain, sucrose esters possess a single sucrose unit in their hydrophilic head and can contain up to eight alkyl chains (as sucrose comprises eight hydroxyl groups that can be esterified) [2,3]. Consequently, SEs usually appear as mixtures of mono-, di-, and polyesters in varying ratios [3–5]. This diversity enhances their applicability, as varying the mixture composition alters the hydrophilic-lipophilic properties of SEs (respectively their hydrophilic-lipophilic balance, HLB) [3]. This versatility makes them suitable for a broad range of products, whether they are oil- or water-based.

Sucrose esters are considered as green surfactants as they are non-toxic and biodegradable [1–7]. Moreover, they have gained significant attention for their diverse beneficial properties including antimicrobial, antioxidant, antitumor, anti-inflammatory, and insecticidal activities [5,8–11]. These esters are both tasteless and odorless, making them suitable for various applications in food [12–14], cosmetics [5], and pharmaceuticals [3–5,15,16]. SEs can be synthesized from cost-effective and renewable sources (sucrose and naturally occurring fatty acid sources) [2,5,17,18], and can also be directly derived from natural products such as fruits, leaves, and other plant parts [8]. These characteristics make SEs excellent candidates not only for replacing synthetic petrochemical surfactants, but also for introducing additional advantages to end products.

In addition to their interesting physiological properties, several studies demonstrate that sucrose esters can form wormlike micelles in the presence of various additives, incl. nonionic surfactants, fatty acids and alcohols, and oils [19–24]. Moreover, several authors have identified intriguing rheological properties in aqueous sucrose stearate solutions in response to temperature variations [25–27].

One of the first studies exploring the phase behavior of sucrose stearate surfactant (70 wt% monoester and 30 wt% di- and triesters content; 70 % stearic and 30 % palmitic fatty acids) in water at various concentrations and temperatures was conducted by Calahorro et al. back in 1992 [25]. In this study, the authors suggested a phase diagram comprising a two-phase region containing undissolved solid and micellar solution for concentrations below 10 wt% and temperatures below 43 °C. Above 43 °C, a transition to a micellar solution at this surfactant level was proposed. No birefringence was observed for these concentrations [25].

The authors characterized the rheological behavior of these systems at 50 °C and demonstrated a power-law decrease in viscosity with shear rate (up to shear rates $\approx 200\ s^{-1}$) for 1 and 2 wt% sucrose stearate solutions [25]. In contrast, more concentrated solutions (2 wt% $< c \leq$ 10 wt%) exhibited two well defined regions in the flow curves. At low shear rate the apparent viscosity remains constant as a function of shear rate for all studied concentrations, whereas above a critical shear rate, dependent on the surfactant concentration, a significant drop in the apparent viscosity with shear rate was observed. These data were well described by Carreau A rheology model [28]. The authors attributed this peculiar behavior to the presence of a micellar structure whose strength increases with surfactant concentration. The appearance of viscoelasticity at concentrations above 2 wt% was explained by the overlapping of micelles, hindering their free movement under flow [25].

The phase behavior of the aqueous solutions of sucrose stearate (77 wt% monoesters, 20 wt% diesters and 3 wt% triesters) was also investigated more recently by Takahashi and Kaneda [27]. These authors proposed a slightly different phase diagram comprising both translucent and turbid regions at temperatures below 48 °C and concentrations ranging from 1 to 8 wt%. Beyond this critical temperature, the samples were asserted to be transparent. The translucent phase at low temperatures was suggested to contain discrete micelles or vesicles, whereas larger molecular assemblies were hypothesized for the turbid phase, although these structures were not analyzed in details [27].

At higher temperatures, the authors observed a peak in the apparent viscosity, calculated from the measured loss modulus at low frequency of oscillations, around 48 °C, followed by a slight decrease at higher temperatures [27]. Notably, even at 60 °C, the calculated apparent viscosities remained significantly higher than those obtained at 20–30 °C. The measured storage modulus in the plateau region at 50 °C was shown to increase with sucrose ester concentration with a power law index of 1.7 which was attributed to the entanglement of a thread-like molecular assemblies present in solution [27]. Similar dependence was found for the apparent viscosity as a function of sucrose ester concentration based on the data provided in Table 1 in Ref. [27], showing that the apparent viscosity also increases with surfactant concentration with a power law index of 1.7. This result diverges from the findings of Calahorro et al. [25], who demonstrated, using similar surfactant, that the apparent viscosity curves remaine independent of concentration up to a critical shear rate value at the same temperature.

Finally, some studies have proposed the formation of multilamellar vesicles or network of vesicles in sucrose stearate solutions at low temperatures and concentrations below 10 wt% [26,30–32]. Direct electron microscopy observations are available in Refs. [31,32] for the aqueous solutions of sucrose stearate surfactants with varying HLB values studied at 25 °C. The authors suggested creation of closed vesicles with diameters ranging from 50 to 600 nm for a mixture containing 40 wt% monoester and 60 wt% di-/tri-/polyesters of sucrose stearate with HLB = 7 [31]. A network of closed vesicles coexisting with other closed vesicles was suggested at 3 wt% concentration of this surfactant. These solutions experienced a typical shear thinning behavior [31]. Additionally, the formation of closed vesicles of two predominant sizes (approximately 25 nm and 200 nm) is proposed for solutions of a more hydrophilic sucrose stearate (composed of 70 wt% monoesters and 30 wt % di-/tri-/polyesters, HLB = 15) at concentrations ranging from 0.01 and 1 wt% [32]. Note that the optimal packing parameter for vesicle formation falls within the range of ½ and 1 [33]. In contrast, wormlike micelles, proposed to be present in such solutions at elevated temperatures by the other researchers [25,27], display a packing parameter between $^1/_3$ and ½ [33]. The specific pathway for this transition remains currently unknown.

This brief literature review demonstrates that a further investigation is needed to enhance our understanding of the temperature dependent molecular arrangement displayed by the biodegradable sucrose ester surfactants, dissolved in water. It should be noted that the existing studies have focused solely on sucrose stearate solutions, leaving uncertainty about whether this peculiar rheological behavior is specific to surfactants, containing a stearate fatty acid residue, or if other factors play a primary role. Therefore, the current study is designed to answer these questions. Moreover, to emphasize the notable contrast between the behavior observed in the current study and the typical behavior exhibited by low molecular nonionic surfactants, a comparison between

them is presented at the end of the paper.

2. Materials and methods

2.1. Materials

In the present study, we used sucrose fatty acid ester surfactant, purchased from TCI Chemicals (product number S0112). According to the specifications provided by the producer, this surfactant should contain at least 75 % palmitic acid chains. The surfactant will be denoted as C_{16}SE throughout the manuscript. A comprehensive analytical analysis was carried out to determine the specific composition of the studied surfactant, see Section 2.2.2 for description of the experimental procedures and Section 3.1 for the results of the performed analyses. Furthermore, Brij 58 (polyoxyethylene (20) hexadecyl ether, denoted as $C_{16}EO_{20}$), purchased from Sigma-Aldrich was used to demonstrate the typical behavior for nonionic surfactants. All surfactant solutions were prepared with deionized water purified by Elix 3 Module, Millipore USA.

The chemicals used for the analytical analyses (gas chromatography, GC and high-performance liquid chromatography, HPLC) were purchased from Sigma-Aldrich and TCI Chemicals and were of analytical grade.

2.2. Experimental methods

2.2.1. Solutions preparation

All studied solutions were prepared by accurately weighting the required surfactant quantity on an analytical balance. Then, the required amount of deionized water was added and the mixture was stirred at a temperature of 77 °C in a sealed container until the surfactant was completely dissolved (ca. 30 min). Afterwards, the solution was transferred to a water bath set at a temperature of 15 °C and allowed to cool for 20 min. The final temperature reached after cooling was ca. 25 °C. The prepared solutions were stored overnight at 25 °C prior conducting further experiments. The concentrations of the solutions ranged from 1 to 5 wt%.

2.2.2. Analytical methods

The type of the esters (mono-/di-/tri-/polyesters) present in the studied C_{16}SE surfactant was analyzed using *high-performance liquid chromatography (HPLC)* analyses performed on a Shimadzu apparatus, equipped with a LC-40DX3 delivery module and ELSD detector operating at 40 °C temperature. An analytical column Waters X-Bridge C18 column (150 x 4.6 mm, 3.5 μm particle size) operating at 45 °C was used for the separation of the different molecular species. Further details about the exact procedure are available in the Supplementary Materials Section S1.1 and in Refs [34,35].

To study the fatty acid chain length distribution in C_{16}SE, we also performed *gas chromatography (GC)* analyses using Agilent 8890 (Agilent Technologies, Santa Clara, CA, USA) equipment. The exact experimental procedure was similar to the one described in Refs [34,35] and is described in details in the Supplementary Materials Section S1.2.

2.2.3. Optical microscopy observations

The optical microscopy observations were performed on AxioPlan and AxioImager.M2m microscopes (Zeiss, Germany). We used transmitted cross-polarized white light, with an additional λ compensator plate placed after the observed specimen and before the analyzer, oriented at a 45° angle with respect to both the analyzer and the polarizer. Under these conditions, the isotropic background have the typical magenta color, whereas the birefringent objects appear with bright colors [36]. The samples were either placed in glass capillaries with a rectangular cross section (width 2 mm and height 0.1 mm), or onto a glass slide and covered with a small glass cover slide when a thinner specimen was needed.

The temperature resolved experiments were performed with a specially designed aluminum thermostatic chamber connected to a thermostat (Julabo CF30). Further details about this experimental set up can be found in Refs [36,37].

2.2.4. Cryo-TEM observation

The specimens used for cryo-TEM observations were prepared with Vitrobot system (FEI, USA) at 100 % relative humidity. Briefly, the bulk samples and the Vitrobot system were pre-heated to the desired temperature for investigation (25, 40 or 55 °C). Afterwards, a drop of the tested solution sample was placed on a holey carbon copper TEM grid, the excess liquid was blotted off with a filter paper and then the sample was plunged into a liquid propane-ethane mixture to form a vitrified specimen. Then the specimen was transferred into a liquid nitrogen and stored in it until further inspection.

The cryo-TEM imaging was performed using a Gatan cryo-specimen holder at JEM2100, JEOL high-resolution transmission electron microscope. An acceleration voltage of 200 kV was used. Micrographs were recorded with the Gatan Orius SC1000 camera.

2.2.5. Rheological measurements

The rheological properties of the solutions were characterized with a rotational rheometer (Anton Paar, MCR-302e). A cone and plate geometry (40 mm cone diameter, 1° cone angle, truncation gap 78 μm) was employed. Three different types of measurements were performed: Flow ramps in which we measured the viscosity of the sample as a function of the applied shear rate at a given pre-determined temperature. The shear rate was varied between 0.1 and 500 s^{-1} in a logarithmical manner. Temperature ramps were also performed for part of the samples. In these experiments, the temperature of the sample was varied at a rate of 1 °C/min. The measurements were conducted at a constant shear rate of 1 s^{-1}. We also performed amplitude sweep oscillatory experiments in which the storage and loss moduli (G' and G'') were determined as a function of the applied shear strain (varied between 0.1 and 1000 %).

2.2.6. DSC measurements

The differential scanning calorimetry (DSC) experiments were performed with Discovery DSC 250 apparatus (TA Instruments, USA). The exact procedure for sample preparation can be found in Ref. [37].

In the present study, we used the following temperature protocol to analyze the samples: The investigated aluminum pan containing the sample (weight ≈ 20–30 mg) was placed in the DSC apparatus at 30 °C. Afterwards, the temperature was decreased to 10 °C with 10 °C/min rate. The sample was equilibrated at this temperature for 10 min and then it was heated up to 65 °C with 2 °C/min rate. Then, a cooling step was performed decreasing the temperature of the investigated sample down to 0 °C at 2 °C/min rate. In some cases, we also performed a second cooling-heating cycle using the same protocol. These experiments gave us qualitative information about the phase transitions occurring upon temperature variation in the samples and quantitative information about the enthalpy of each phase transition.

2.2.7. NMR analysis

The NMR study was carried out on a Bruker Avance III HD spectrometer 500 MHz spectrometer (Rheinstetten, Germany) equipped with a high-resolution broadband probe-head with Z gradient. Experiments were conducted at 25 °C, 40 °C and 50 °C. Prior to these measurements, we added 0.1 ml of deuterium oxide (99.8 atom % D) with TMSP-Na-2,2,3,3-d_4 as internal standard (0 ppm) to 0.5 ml of the prepared sucrose ester solution. Topspin 3.6.5 software package (Bruker) was used for spectrum collection and data analysis.

2.2.8. SAXS/WAXS measurements

The structure of the investigated sample was also analyzed using X-ray scattering system (Xeuss 3.0, Xenocs, France) equipped with Eiger2 4 M detector (Dectris Ltd., Baden Deattwil, Switzerland), CuKα X-ray source (λ = 0.154 nm) and slit collimation system. The images were

detected at different sample-to-detector distances varied between 300 and 3500 mm depending on the *q*-range of interest for the particular sample.

Samples with low viscosities were enclosed into a vacuum tight thin special glass capillary (WJM Glass, Germany) with an outer diameter of 1 mm and wall thickness of 10 μm. The viscous samples, were analyzed in stainless steel flat washers. The investigated sample was mounted in the washer using two adhesive Kapton tapes. The temperature of the samples was controlled with HFSX350 high-temperature stage, equipped with a T96 temperature controller and an LNP96 liquid nitrogen pump, all products of Linkam Scientific Instruments Ltd., UK. The temperature in the samples was varied with 1 °C/min rate. The acquisition time for a single image varied between 300 and 1200 s depending on the sample-to-detector distance used. The scattered intensity was normalized to the incident beam intensity and was corrected for the background scattering from sample holder. For this, we measured the scattering signal coming from a purified water enclosed either into a glass capillary or into a stainless steel washer. The SASView software was used for the SAXS data analysis. A detailed explanation about the employed models and the parameters used in them is presented in Supplementary Materials Section S2.

2.2.9. Centrifugation

To analyze precisely all different entities, present in the solution at various temperatures, we performed also centrifugation experiments which allowed us to separate the initial sample into few individual layers which were further analyzed separately. Two different centrifugation procedures were used. The samples were separated either by using 15 min centrifugation at 20 000 g acceleration with refrigerated centrifuge Sigma 3 K15, Sigma, Germany or by using 30 min centrifugation at 165 000 g with ultracentrifuge Eppendorf CP100NX, equipped with a P70AT rotor. The centrifugations were performed at 25 °C. Eppendorf microtubes ® with volume 1.5 ml and a conical bottom were used for centrifugation at 20 000 g acceleration, see the picture in Fig. 4a below. About 1.4 ml sample was added to each microtube. The height of the liquid was approximately 3.3 cm. Polycarbonate tubes with a volume of 33 ml and an inner diameter of 2.3 cm were used for the ultracentrifugation. In this case ca. 25 ml sample was added to each tube before the centrifugation (liquid height ≈ 7 cm).

3. Experimental results and discussion

3.1. Chemical analysis of the investigated sucrose ester

To comprehensively interpret the obtained experimental results, a precise understanding of the chemical composition of the investigated surfactant is essential. For that reason, various chemical analyses were conducted, as detailed in Section 2.2.2 above and in Supplementary Materials Section S1. The results of these analyses showed that the studied sucrose palmitate (referred as C_{16}SE throughout the text) comprises approximately 80 ± 4 % palmitic acid chains (C_{16}) and ca. 20 ± 4 % stearic acid chains (C_{18}), see Supplementary Figure S1. Additionally, HPLC analysis indicated that around 80 ± 5 % of the molecules present are monoesters, while the remaining 20 ± 5 % encompass higher esters, with the diesters fraction being predominant, see Figure S1 in Supplementary Materials. This relative complex mixture of molecules should be considered when interpreting all other experimental results.

3.2. Characterization of the (complete) sucrose ester solutions

3.2.1. Solution appearance at different temperatures

Fig. 1a illustrates the macroscopic and microscopic appearance of the C_{16}SE solution at different temperatures. As can be seen, significant changes occur with temperature variations. At 25 °C, the C_{16}SE solutions exhibit significant turbidity with numerous thread-like structures visible under the microscope. Some of these structures display birefringence under polarized light, indicating the presence of well-ordered lamellar structures. Significant changes appear in the sample upon heating, see Fig. 1, Supplementary Figure S2 and Supplementary Movie 1. The thread-like structures start to gradually diminish when the temperature is increased above ca. 38 °C, resulting in a fully isotropic appearance around 42 °C (at least at the microscopic level). Further heating leads to the formation of spherical droplets. The macroscopic observations align well with the microscopic images, as demonstrated by the inset pictures included in Fig. 1a.

To confirm that the observed changes result from a melting phase transition proceeding in the solution, we conducted a DSC experiment, see Fig. 1b. A broad endothermic peak in the temperature range of 30 to 45 °C was observed when the 5 wt% C_{16}SE solution was heated. The enthalpy of the peak was $\Delta H_m \approx 1.69 \pm 0.03$ J/g (data derived from three independent experiments). Considering that the water does not undergo any phase transitions within this temperature interval, the

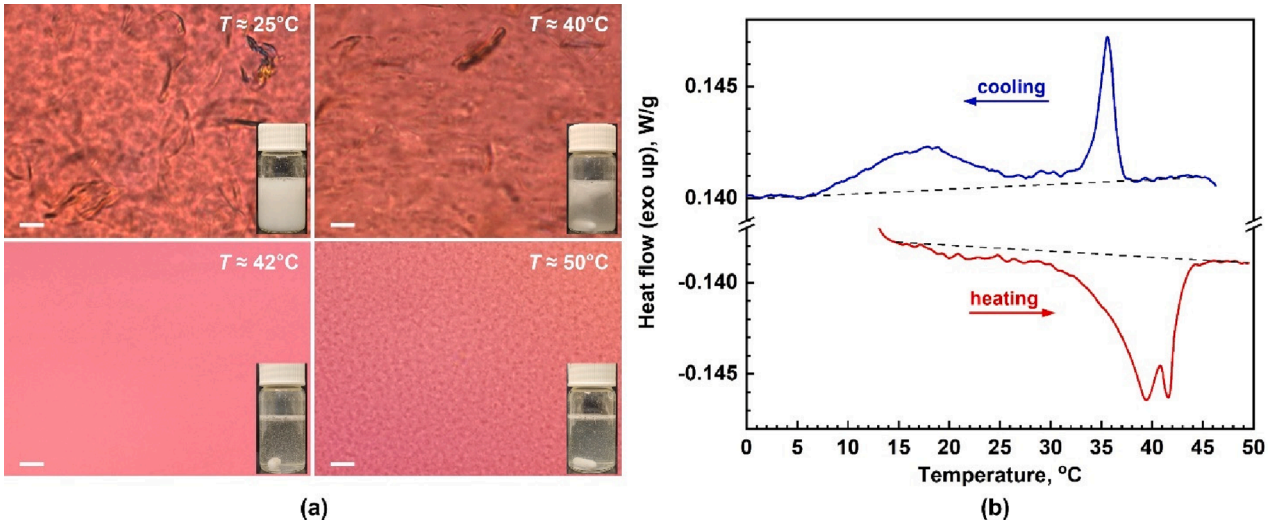

Fig. 1. Phase behavior of 5 wt% C_{16}SE solution. (a) Optical microscopy pictures, obtained at different temperatures. Inset: macroscopic appearance of the sample. Scale bars = 10 μm. (b) DSC heating (red curve) and cooling (blue curve) thermogram of the solution. Dashed lines show the baseline and are guide to the eye only. (For interpretation of the references to color in this figure legend, the reader is referred to the web version of this article.)

actual phase transition enthalpy for the sucrose ester surfactant was estimated to be $\Delta H_{SE,m} \approx 33.8 \pm 0.6$ J/g. Two distinguishable maxima were observed in the heating thermogram at $T \approx 39.5$ °C and 41.7 °C. These peaks likely result from the presence of diester molecules arranged in different supramolecular structures, see the discussion in Section 3.4 below.

Upon subsequent cooling of the same sample, two distinct peaks are clearly observed, see the blue curve in Fig. 1b. Nevertheless, the initial structure is not entirely restored. The exothermic peak has a significantly smaller enthalpy ($\Delta H_c \approx 1.08 \pm 0.02$ J/g, $\Delta H_{SE,c} \approx 21.6 \pm 0.4$ J/g) compared to the endothermic peak enthalpy observed during the heating step.

3.2.2. *Rheological properties of the solutions at different temperatures*

The changes in the visual appearance of the sample correspondingly influenced its rheological behavior, aligning with the results available in the literature for sucrose stearate surfactant [27]. To the best of our knowledge no such results are available in the literature for sucrose palmitate, which is investigated in the current study. Fig. 2 illustrates the viscosities of solutions prepared with C_{16}SE surfactant solutions with concentrations between 1 and 5 wt% at different temperatures. A viscosity peak is observed in the solutions at ca. 40 °C, see Fig. 2d. This temperature closely aligns with the phase transition temperature, revealed by the DSC experiment, see Fig. 1b. Lower viscosities are measured at higher or lower temperatures, however, the flow curves obtained at 25 °C and 50 °C exhibit distinctive behavior.

Solutions containing up to 3 wt% C_{16}SE behave as Newtonian liquids at 25 °C, with viscosity slightly increasing as the surfactant concentration rises. In contrast, the 5 wt% sucrose palmitate solution displays non-Newtonian shear thinning behavior at 25 °C. It exhibits gel-like behavior, transitioning to a more fluid-like under high shear rates. The observed behavior is attributed to the increase of the number of undissolved thread-like structures in the solutions upon increase of the surfactant concentration. Note that these systems are homogeneous and their viscosity measurements are with good reproducibility.

The increase of temperature to 40 °C leads to a significant increase in the viscosity of the solutions by approximately 3 orders of magnitude, Fig. 2b. Even at the lowest concentration of 1 wt%, a zero-shear viscosity of ca. 1 Pa.s is measured at 40 °C, whereas the zero-shear viscosity of the same solution at 25 °C is $\eta_{25°C} \approx 2.7$ mPa.s. Two distinct regions are observed in the flow curves obtained at 40 °C: a plateau region where the viscosity remains relatively constant with shear rate, for $\dot{\gamma} \lesssim 0.1$ s^{-1}, followed by a steep decrease in viscosity as the shear rate increases. The power law index for viscosity decrease in the second region is $\approx 0.9 \pm 0.02$ and slightly increases with the surfactant concentration (it is around 0.88 for 1 wt% C_{16}SE and approximately 0.92 for 5 wt% C_{16}SE).

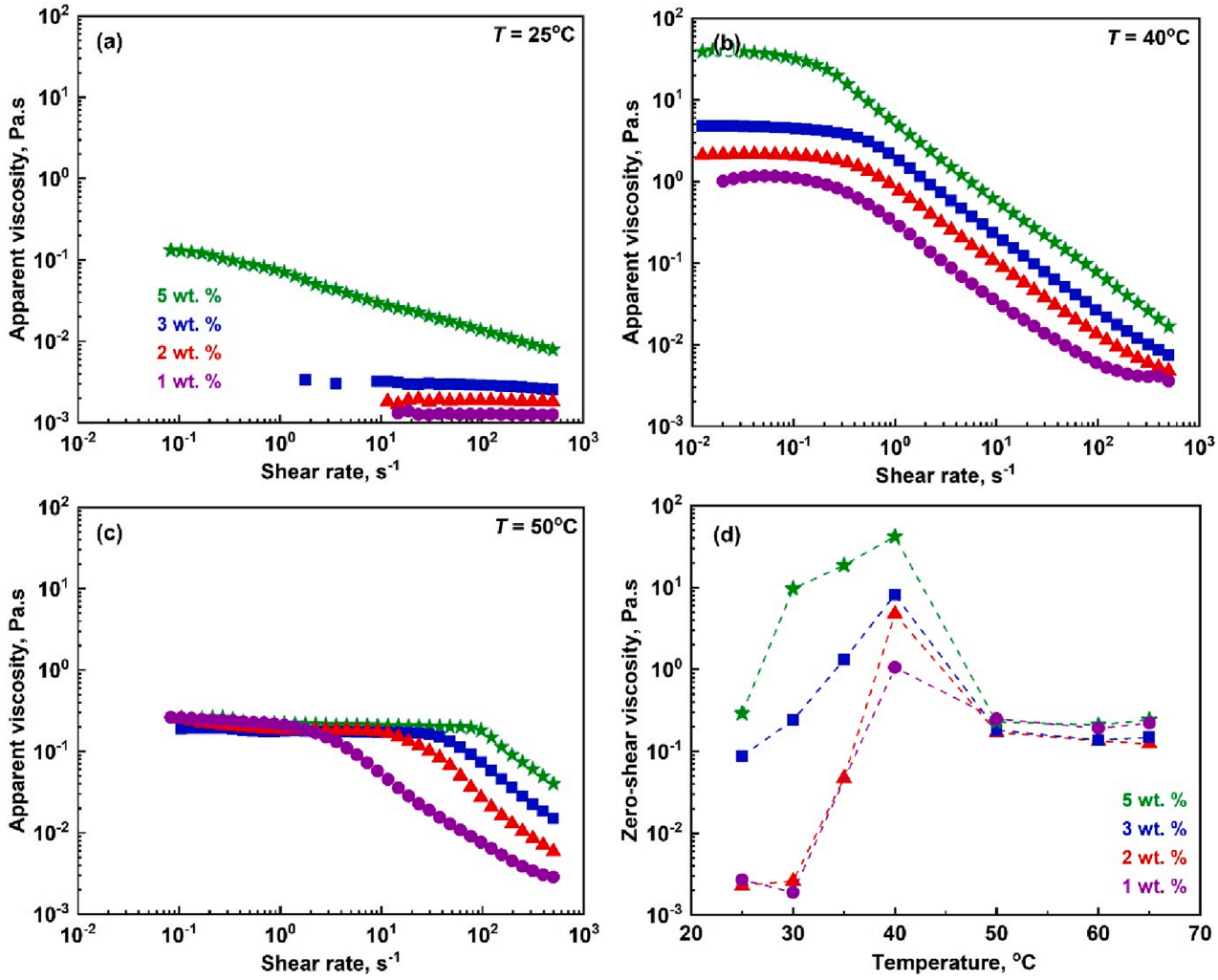

Fig. 2. Rheological behavior of the C_{16}SE solutions. (a-c) Flow curves measured at different constant temperatures: (a) $T = 25$ °C; (b) $T = 40$ °C; (c) $T = 50$ °C. (d) Zero-shear viscosity as a function of the temperature. In all graphs the different symbols denote the C_{16}SE concentrations: 1 wt% – purple circles; 2 wt% – red triangles; 3 wt% – blue squares; 5 wt% – green stars. (For interpretation of the references to color in this figure legend, the reader is referred to the web version of this article.)

We note that although similar, the rheological properties of solutions containing interwoven wormlike micelles are not completely identical to those seen in the present study. In systems with entangled wormlike micelles, the rheological response at high shear rates is expected to be inversely proportional to the shear rate, *i.e.* $\eta \propto \dot{\gamma}^{-1}$ [29,38,39], whereas in the current case it is $\eta \propto \dot{\gamma}^{-0.9}$. This observation suggests the possible presence of entangled wormlike micelles in the C_{16}SE solutions, along with additional supramolecular structures.

When the temperature exceeds 40–45 °C, the rheological properties of the solutions change once again, see Fig. 2c. Although an overall decrease in viscosity is observed across all studied concentrations, the solutions do not revert to their rheological properties observed at lower temperatures. Instead, a plateau region emerges, where viscosity remains independent of the sucrose palmitate concentration ($\eta \approx 0.22 \pm 0.02$ Pa.s) at low shear rates. This plateau region is followed by another region, where viscosity decreases steeply with increasing shear rate. The critical shear rate, at which the transition between these two regions occurs, depends on the C_{16}SE concentration: it is $\dot{\gamma}_{crit} \approx 2\ s^{-1}$ for 1 wt% C_{16}SE, and increases to 11 s^{-1}, 35 s^{-1} and 85 s^{-1} for 2, 3, and 5 wt% C_{16}SE solutions, respectively.

The concentration independent plateau viscosity, observed at temperatures higher than 50 °C, is most probably associated with the presence of an interconnected branched micellar network, which occupies the solution volume and determine its viscosity at low shear rates. The observed increase in critical shear rate values with surfactant concentration correlates with the enhanced mechanical strength of the network. To demonstrate this, we conducted amplitude sweep experiments (at 1 Hz frequency) to measure the viscoelastic response of the solutions. Fig. 3 illustrates the experimental results about the storage and loss moduli of the investigated solutions. These results show that the viscoelastic properties of the solutions are influenced by both temperature and surfactant concentration. At 25 °C, Fig. 3a, the 2 wt% solution behaves as a typical viscous liquid, with the storage modulus *G*' being smaller than the viscous modulus *G*''. In contrast, the 5 wt% solution exhibits higher elasticity with *G*' > *G*'' up to ca. 5 % strain, beyond which the two curves intersect, and the loss modulus surpasses the storage modulus.

At 40 °C, Fig. 3b, the moduli increase significantly for both 2 and 5 wt% solutions and change their strain dependence. Throughout a wide strain range, *G*' and *G*'' remain relatively steady, with *G*' slightly surpassing *G*''. Beyond a critical shear strain, the storage modulus sharply declines and the loss modulus becomes higher than the storage modulus. As the temperature increase further, Fig. 3c, the system behavior shifts once more. The *G*' and *G*'' moduli attain relatively constant values independent of the applied shear strain (up to 100 % strain) and nearly independent of the surfactant concentration. Therefore, the storage moduli are higher than the loss moduli at low temperatures, whereas above the phase transition temperature the storage moduli become around 10 times lower than the loss moduli and do not depend on the surfactant concentration (in the studied range) which is a very unusual behaviour explained below.

The presented results highlight the intricate behavior exhibited by the sucrose palmitate solutions. To understand the observed phenomena at a molecular level, it is crucial to acknowledge that the studied sucrose palmitate surfactant consists of mixtures of mono- and di-esters with varying fatty acid residues, as explained in Section 3.1. However, as high purity sucrose monoesters and diesters are unavailable, we sought to understand the role of different molecular species by attempting to separate the prepared solutions through centrifugation.

3.3. Characterization of the sucrose ester solutions after centrifugation

The aqueous solution of C_{16}SE contains undissolved thread-like structures at 25 °C, as seen in Fig. 1a. These structures most probably consist of the more hydrophobic diester molecules, which exhibit lower solubility compared to monoesters. To confirm this hypothesis, we centrifuged sample of the prepared solutions to isolate and analyze these thread-like structures in details. Fig. 4a illustrates the appearance of the sample after 15 mins of centrifugation at an acceleration of 20 000 g.

Upon centrifugation, three distinct layers were obtained, referred to as the "*top*", "*middle*", and "*bottom*" layer in the following discussions. The *top* layer (serum) exhibited low viscosity and was slightly opalescent at 25 °C. The *middle* layer displayed increased viscosity and much higher turbidity than the serum, whereas the *bottom* layer (sediment) appeared opaque with significantly higher viscosity than the other two layers. Chemical analysis of these layers (performed by HPLC, see Supplementary Materials Section S1.1) showed that the *top* layer predominantly contained monoesters (monoesters to diesters ratio ≈ 7.5:1), whereas the concentration of the diesters was significantly increased in the opaque *bottom* layer (monoesters to diesters ratio ≈ 2:1). The *middle* layer exhibited a similar monoester to diester ratio as the one found in the original sample before centrifugation (monoesters to diesters ≈ 4:1), but with a slightly increased concentration of the longer C_{18}-monoesters. This *middle* layer had similar properties to those described in Section 3.2 above. Therefore, the subsequent two sections will describe in details the behavior of the *top* and *bottom* layers only.

3.3.1. Transparent layer (top layer/serum)

Various analyses were conducted to characterize the composition, macroscopic and microscopic structure, as well as the rheological behavior of the transparent *top* layer separated from the C_{16}SE solutions after centrifugation.

The total surfactant concentration contained within the serum separated from 5 wt% C_{16}SE solution was estimated to be ca. 4 wt% (from both DSC and HPLC results). The chemical analyses performed on five independently prepared serums showed a predominant presence of monoesters in them. The monoester content was determined to be ca. 87 ± 4 %, whereas the diesters constituted around 13 ± 4 %. Consequently,

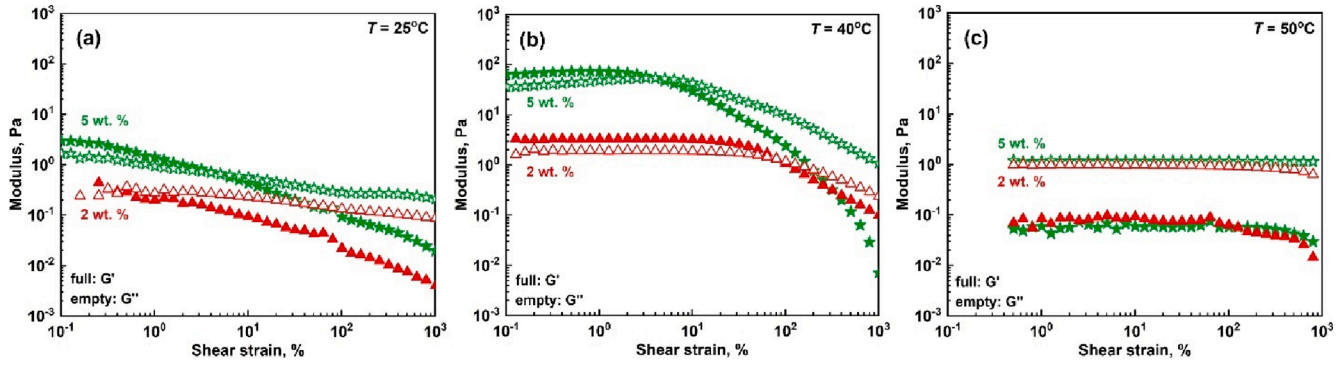

Fig. 3. Storage (full symbols) and loss (empty symbols) moduli measured for 2 wt% (red) and 5 wt% (green) C_{16}SE solutions at different temperatures: (a) $T = 25$ °C; (b) $T = 40$ °C; (c) $T = 50$ °C. (For interpretation of the references to color in this figure legend, the reader is referred to the web version of this article.)

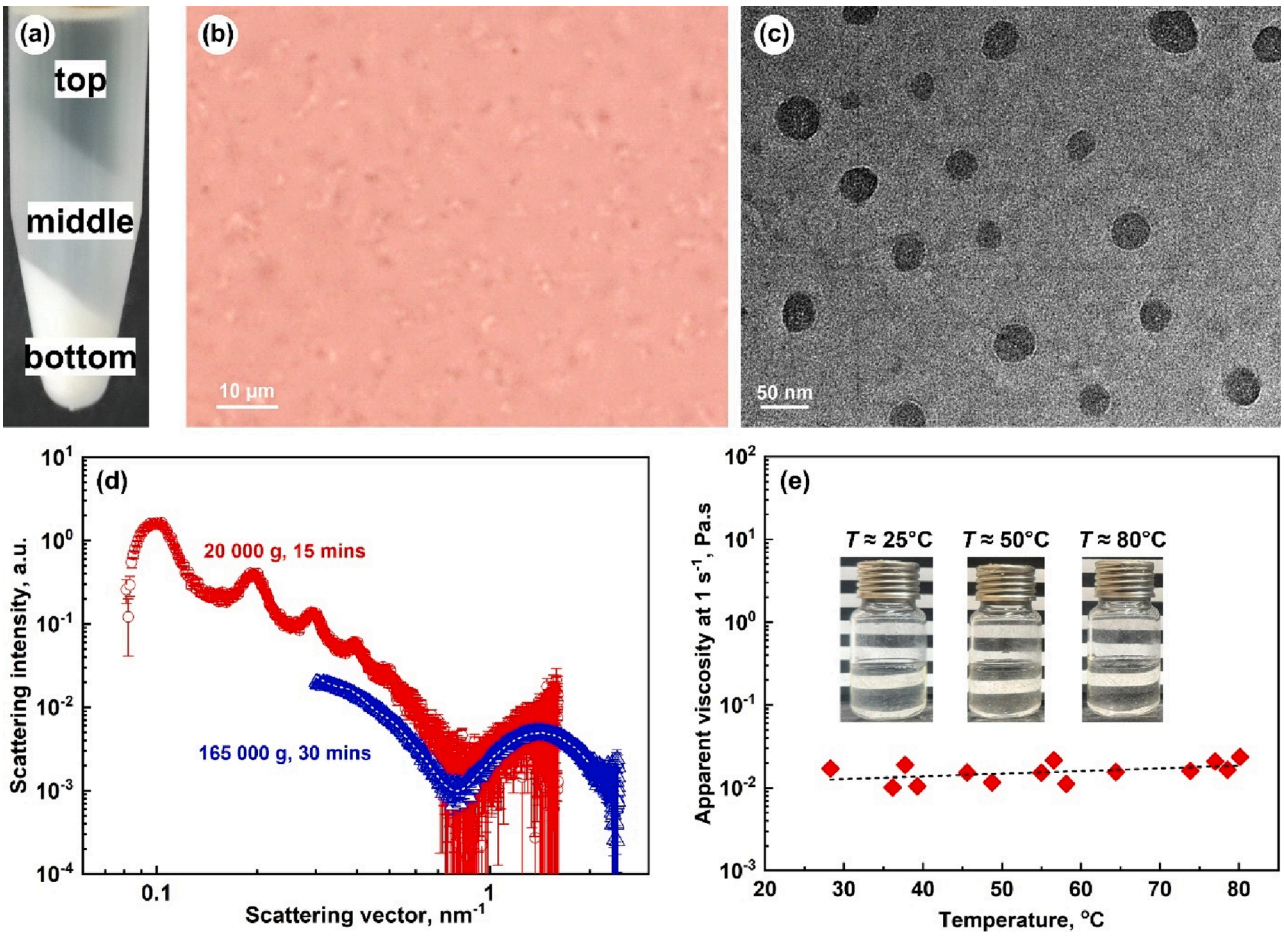

Fig. 4. Analysis of *top* layer separated after centrifugation from 5 wt% C_{16}SE solution. (a) Image showing the three different layers obtained after 15 min. centrifugation at 20 000 g. (b) Optical microscopy image of the *top* layer. Small entities are seen which have sizes below the diffraction limit. The sample was prepared at 25 °C. (c) Cryo-TEM image of the *top* layer. Particles with characteristic size ≈ 44 nm are observed. (d) SAXS spectra obtained at 25 °C from the top layers separated after 15 min. centrifugation at 20 000 g (red symbols) or 30 mins centrifugation at 165 000 g (blue symbols). The white dashed line represents the model fit for the ultracentrifuged sample, see Supplementary Materials Section S2 and the main text for more details. (e) Apparent viscosity as a function of temperature for the *top* layer sample separated after 15 min. centrifugation at 20 000 g. The dashed line is guide to the eye only. Inset: appearance of this sample at different temperatures. (For interpretation of the references to color in this figure legend, the reader is referred to the web version of this article.)

the behavior of this serum is expected to be primarily determined by the sucrose monoesters.

The optical microscopy observations on the serum showed a picture without any visible thread-like structures, see Fig. 4b. The sample contained small structures below the resolution limit, making detailed visualization challenging. To investigate further these structures, cryo-TEM imaging was performed, see Fig. 4c and Supplementary Figure S3. Unexpectedly, the cryo-TEM images revealed the presence of numerous relatively monodisperse particles. Note that these particles could not be vesicles, as previously suggested for more hydrophobic sucrose stearate solutions in Refs. [31,32], given their isotropic contrast throughout the entire particle, without visible concentric circles characteristic of multilamellar vesicles, or a darker periphery and brighter inner part observed for unilamellar vesicles [40,41]. Furthermore, the particles resembled the triacylglyceride nanoparticles observed in Ref. [42]. Hence, the presently observed particles composed from the less soluble diglyceride molecules, potentially stabilized by adsorbed monoester molecules on their surfaces. This hypothesis was further validated by the results obtained from the structural SAXS experiment, see below.

To further characterize the observed diglyceride particles, found in the serum obtained after centrifugation of the initial surfactant solution, we measured their sizes and created a size distribution chart, see Figure S3 in Supplementary Materials. The average volume-surface particle diameter, $d_{32} = \sum_i d_i^3 / \sum_i d_i^2$, where d_i represents the measured particle diameter, was determined to be $d_{32} \approx 42$ nm. This value is similar to the average diameter calculated when the drop size distribution is described by a Gaussian distribution function, yielding $d_{ave} \approx 44$ nm, with a standard deviation $\sigma \approx 9$ nm. The polydispersity index of these particles is $\mathrm{PdI} = (\sigma/d_{ave})^2 \approx 0.04 < 0.1$, indicating that they are highly monodisperse [43].

To further investigate the structures present in the solution, next we performed SAXS experiments. The scattering curve for the *top* layer, separated after 15 min. centrifugation at 20 000 g, is presented with red symbols in Fig. 4d. The analysis of the obtained signal revealed two distinctive structures: diester particles and slightly elongated ellipsoidal micelles.

The diester particles were observed with a series of peaks appearing at a scattering vector $q < 0.5$ nm^{-1}, with a peak maxima ratio of 1:2:3… The primary peak was observed at $q \approx 0.1$ nm^{-1}, with the first four reflections clearly visible in the spectrum. This result confirms the highly monodisperse nature of the diester particles, as otherwise the form factor would be smeared, and the scattering function would not exhibit such distinguishable peaks [44,45]. Additionally, the analysis of the peak positions, assuming the scattering is due to spherical objects in the sample, indicates a characteristic diameter of ≈ 60 nm, which is within the range of particle sizes observed in the cryo-TEM images.

In a separate experiment, we investigated the changes in the SAXS

spectra of the serum upon heating, see Supplementary Fig. S4a. The results showed a continuous decrease in particle size as temperature increased. Notably, the peaks indicating particles presence completely vanished at 43 °C. This temperature coincides with the phase transition temperature, detected in the optical microscopy observations. This provides a direct evidence that the molecules constituting the particles undergo a phase transition and rearrangement when the temperature exceeds ca. 43 °C. This endothermic transition was further confirmed in a DSC experiment, where a melting peak with a maximum at $T \approx 40$ °C and an enthalpy of ≈ 1 J/g was detected for this serum, see Supplementary Fig. S4b.

To unambiguously confirm that the scattering peaks at $q < 0.5$ nm^{-1} are related to the presence of diester particles, we performed an additional experiment. In this experiment, instead of using relatively mild centrifugation conditions, we utilized an ultracentrifuge for 30 mins at an of acceleration 165 000 g. Following this centrifugation, once again, three distinct layers were obtained (see Supplementary Fig. S4b). Chemical analysis of the serum separated after the ultracentrifugation (by the HPLC method) revealed a significant decrease in diesters content. The monoesters-to-diesters ratio in the ultracentrifuged serum became ca. 22:1, whereas in the initial *top* phase it was ca. 7.5:1.

The SAXS analysis of the serum, obtained after ultracentrifugation, demonstrated the presence of ellipsoidal micelles only, with no observable scattering peaks from the spherical diester particles, see blue curve in Fig. 4d. Additionally, no peaks were observed also in the DSC heating thermogram of this sample, see Supplementary Fig. S4b. This unambiguously shows that the DSC melting peaks observed between ca. 30 and 45 °C when the full sample is investigated (Fig. 1b), are caused by the phase transition proceeding in the diester molecules. The SAXS, DSC and HPLC results show that the diester particles were fully separated from the serum obtained after ultracentrifugation, resulting in a significantly reduced overall diester content. Additionally, the serum separated after ultracentrifugation was completely transparent confirming the absence of objects that could scatter light, see the insets in Supplementary Fig. S4b. The total surfactant concentration determined by the HPLC analysis for this serum was ca. 2.5 wt%. The negligible amount of diester molecules (ca. 0.1 wt%) present in the ultracentrifuged serum are arrange together with the monoester molecules into ellipsoidal micelles.

In all SAXS spectra obtained from the separated serums, a consistent presence of a peak indicative of micelles was observed, regardless of the existence of diester particles. Analysis of this peak revealed micelles with a slightly elongated ellipsoidal shape with an inner radius $R \approx 2.1$ nm, shell thickness ≈ 0.56 nm, and aspect ratio ≈ 2.2. Further details about the SAXS modeling employed are available in Supplementary Materials Section S2, see also the dashed curve in Fig. 4d. We note that the determined micelles sizes are in a good agreement with the experimentally measured values for micelles sizes formed from very diluted solutions (concentration ≈ 0.06 wt%) of 6-*O*- and 6′-*O*-hexadecylsucroses, where previous research identified spherical micelles with diameters of 5–7 nm [46].

To assess how the significantly reduced content of diesters affects the bulk properties of the sample upon heating, we conducted rheological measurements, see Fig. 4e. The measured viscosity remained consistently low (with a minimal increase in the values upon heating) across the entire temperature range of 25 to 80 °C. This result confirms that the observed viscosity increase in the full sucrose ester solutions is mainly governed by the presence of diester molecules and their rearrangement in response to temperature variations.

3.3.2. Bottom layer (sediment)

The sediments separated after centrifugation appear as highly viscous opalescent gels, see the image shown in Fig. 4a. The chemical analysis of the sediment showed that the monoesters and diesters percentage content was ≈ (2.2 ± 0.7): 1, *i.e.* the diesters were concentrated in this fraction as compared to the initial solution. The optical microscopy observations of the sediment revealed numerous thread-like structures, see Fig. 5. They were similar to those seen in the whole sample before the centrifugation, but with an increased number.

The SAXS analysis, Fig. 5a, demonstrated the presence of particles, similar to those observed in the serum, by a series of peaks, detected at scattering vector $q < 0.5$ nm^{-1}. In addition, the SAXS spectra showed a presence of inner molecular arrangement into lamellar structure with a characteristic *d*-spacing, $d \approx 4.26 \pm 0.02$ nm at 25 °C. This thickness is slightly bigger than the one which was measured for the pure surfactant (without added water), $d \approx 3.96 \pm 0.02$ nm, demonstrating a bounded water layer with thickness of ca. 0.3 nm situated between the individual lamellae. Furthermore, the WAXS spectra revealed a small peak at $q \approx 15.2$ nm^{-1} ($d \approx 0.41$ nm) which is characteristic for lamellar phases containing molecules with highly ordered tails. This phase is usually denoted as L_β or alternatively referred to as "gel phase" [47,48]. Some micelles were also detected in these samples as shown by the halo observed between ca. 1 and 3 nm^{-1} in the SAXS spectra. The cryo-TEM imaging of these samples, see Supplementary Fig. S5a, showed that each thread is composed of partially fused network of diester particles, which co-existed with some individual particles, identical to those seen in the *top* layer, in agreement with the results obtained by the optical microscopy and scattering experiments.

A shear-thinning behavior with $\eta \propto \dot{\gamma}^{-0.88}$ at shear rates $\dot{\gamma} \leq 0.5$ s^{-1} which changed to $\eta \propto \dot{\gamma}^{-0.54}$ for $\dot{\gamma} > 10$ s^{-1} was observed for the sediment, see Fig. 5b. This rheological behavior is related to disruption of the internal structures upon shear which leads to significant decrease in the measured viscosities.

Next, we studied the properties of the sediment layer upon heating, Fig. 6. Note that they are expected to be distinguishably different from those observed in the 5 wt% C_{16}SE solution or for the separated *top* layer, as the monoester to diester ratio in the sediment is quite different in all these cases: ca. 80:20 for the full sample; 87:13 for the serum separated after centrifugation, and 69:31 for the sediment.

The sediment did not change significantly its appearance when heated from 25 to 37 °C, compare pictures shown in Fig. 5b and 6a. However, the thread-like network disappeared when the temperature was increased further. In the same time, lamellar structures occupying the entire optical field emerged at $T \approx 38.6$ °C. This indicated that although the "fibers" had disappeared, the lamellar structure was still preserved. Another change was observed once the temperature approached 43 °C. The colorful structure started to disappear, transforming into numerous droplets. These drops seemed to have ultralow interfacial tension, as they coalesce easily with each other and were not perfectly spherical. Many droplets exhibiting some faint colors were still observed even at 55–60 °C, see Fig. 6a.

The described changes in the appearance of the sample are related to an endothermic phase transition which was directly observed in DSC and SAXS/WAXS experiments, see Fig. 6b,c. The measured enthalpy of this phase transition was significantly higher (by more than 3 times) compared to that of the 5 wt% solution before centrifugation, $\Delta H_{sed} \approx 5.4 \pm 0.4$ J/g. The endothermic peak was relatively narrow and had a maximum at $T \approx 41.8 \pm 0.1$ °C.

The structural information, obtained from the SAXS/WAXS experiments upon heating, gave us additional information about the observed transitions and molecular rearrangement proceeding in the sample. The lamellar structure with characteristic spacing $d \approx 4.26 \pm 0.02$ nm observed at $T = 25$ °C, Fig. 5a, remained present up to $T = 43$ °C. However, the peaks showing the presence of spherical particles started to vanish even before that at $T = 40$ °C and became completely absent when the temperature approached 42 °C, see Fig. 6c. In addition, when the temperature surpassed 43 °C, the WAXS peak disappeared, demonstrating that the observed endothermic phase transition is in fact related to the fluidization of the hydrocarbon tails of the diesters and formation of the L_α phase.

This transition was accompanied by a shift of the SAXS peaks toward

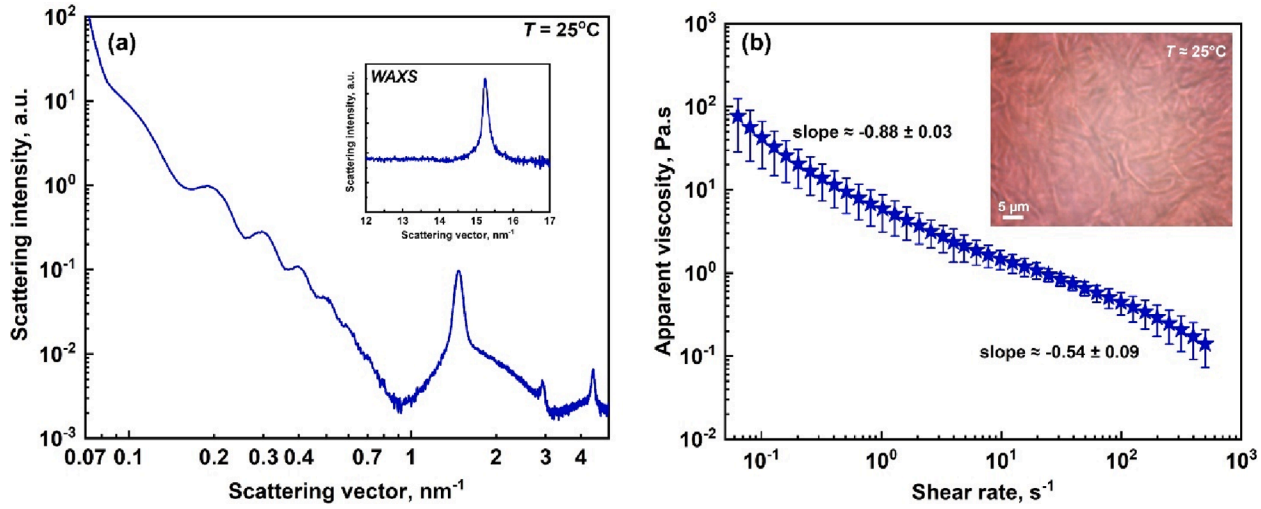

Fig. 5. Characterization of the sediment obtained after centrifugation of 5 wt% C_{16}SE solution at $T = 25$ °C. (a) SAXS spectra of the sediment. Inset: WAXS spectra. (b) Apparent viscosity as a function of the shear rate. Error bars represent the standard deviation calculated from the results obtained in 4 independently performed experiments. Inset: Optical microscopy image in polarized light. Numerous thread-like structures are observed. Scale bar = 5 μm.

lower scattering vectors, *i.e.* larger interlamellar spacings in the bilayer structure. The shift was from $d \approx 4.26$ nm to $d \approx 5.36$ nm at $T > 43$ °C. The observed thickness increase was related to the disordering of the tails and inclusion of additional water molecules in-between the individual lamellae. We note that the thickness increased by ca. 0.2 nm once the L_β-to-L_α phase transition took place in the anhydrous sample, see Supplementary Figure S6. Therefore, the additional 0.9 nm bilayer thickness increase observed in the studied sediment is due to the inclusion of water molecules between the lamellae.

Increasing the temperature above 43 °C led to an increase in the diffusive peak, showing the presence of micelles. Interestingly, two peaks appeared at lower scattering vectors, where the peaks demonstrating the presence of diester particles were observed at lower temperatures. These peaks, with maxima at $q \approx 0.23$ nm^{-1} and at $q \approx 0.45$ nm^{-1} at $T = 44$ °C, shifted toward smaller q-values upon heating but remained visible even at $T = 85$ °C, see Fig. 6c. In real space, these peaks correspond to objects with a characteristic radius of ca. 30 nm. These could be either multilamellar vesicles or, more likely, small spherical droplets primarily composed of excess diester molecules which not incorporated into micelles with monoesters, as the number of diester molecules exceeds the capacity for proper packing within the micelles.

Furthermore, the L_β-to-L_α phase transition and the related structural changes resulted in a significant viscosity decrease as shown in Fig. 6d,e. Once the surfactant tails transitioned to a fluid state, the viscosity decreased more than 10 times and at $T = 50$ °C the power law index decreased to $\eta \propto \dot{\gamma}^{-0.19}$. However, even at this temperature the viscosity of the solution remained around 1 Pa.s due to the relatively high concentration of sucrose ester surfactant and the presence of non-spherical micelles. The sediment viscosity data was obtained by directly measuring properties of samples separation via centrifugation. These sample behaved like gels and were not diluted before the experiments.

3.4. Phase behavior of sucrose palmitate solutions and typical nonionic/anionic surfactants – discussion

3.4.1. Role of monoesters to diesters ratio in sucrose palmitate solutions

The structural characterization results for the full C_{16}SE solution before centrifugation are presented in Fig. 7. A schematic representation of the observed molecular rearrangements upon temperature variation is shown in Fig. 8. These results align well with those obtained from experiments with separate fractions presenting a joint picture from them. In particular, at low temperature (25 °C), the full solution showed the presence of both spherical particles with a characteristic size ≈ 60 nm, along with micelles and lamellar phases with characteristic bilayer thickness of $d \approx 4.27$ nm. When the temperature increased to 40 °C, the particle nearly disappeared, and there was a significant increase in the peak showing the presence of micelles, as seen by comparing the blue and green SAXS spectra for q between ca. 0.8 and 2 nm^{-1}. The wormlike micelles were clearly visualized under cryo-TEM, see Fig. 7b. At 50 °C, the lamellar peak and the peaks showing the presence of particles vanished completely, leaving only the micellar peak in the spectra. No further changes were observed in the SAXS spectra when the temperature was increased to 60–70 °C.

The obtained results are in a good agreement with the measured NMR spectra as well, see Fig. 7e. In particular, the peaks in the range of 0.5–3 ppm, corresponding to the ^{1}H atoms in the hydrocarbon tails, show a significant increase in area when the temperature is increased, area ≈ 1.03×10^7 at 25 °C, 2.24×10^7 at 40 °C, and 2.28×10^7 at 50 °C (measured in absolute points at constant receiver gain). A similar, though smaller increase is also observed for the peaks from the ^{1}H atoms in the hydrophilic heads, area ≈ 1.5×10^6 at 25 °C, 1.8×10^6 at 40 °C, and 1.5×10^6 at 50 °C. Furthermore, no chemical shifts are observed in the NMR spectra, demonstrating that the local electronic environment of the atomic nuclei within the molecules remains consistent within the studied temperature range.

The experimental results highlight the primary role of the sucrose monoesters to diesters ratio over the observed molecular rearrangements. These findings can be explained based on the specific value of this ratio:

I. Monoesters ≫ diesters

This ratio is observed in the *top* phase (serum) separated after ultracentrifugation, where the obtained ratio was ca. 22:1 at a total surfactant concentration of ca. 2.5 wt%. In this case, the monoesters form slightly elongated ellipsoidal micelles with an inner radius $R \approx 2.1$ nm, a shell thickness ≈ 0.56 nm, and an aspect ratio ≈ 2.2. A limited number of diester molecules are incorporated within these micelles. The resulting solution is completely transparent and has very low viscosity, which change minimally upon heating.

II. Monoesters: Diesters ≈ 2.2: 1

This monoester-to-diesters ratio was obtained when the initial surfactant solutions were centrifuged and the sediment layer was separated from the rest of the sample. The concentrated sediment obtained from a

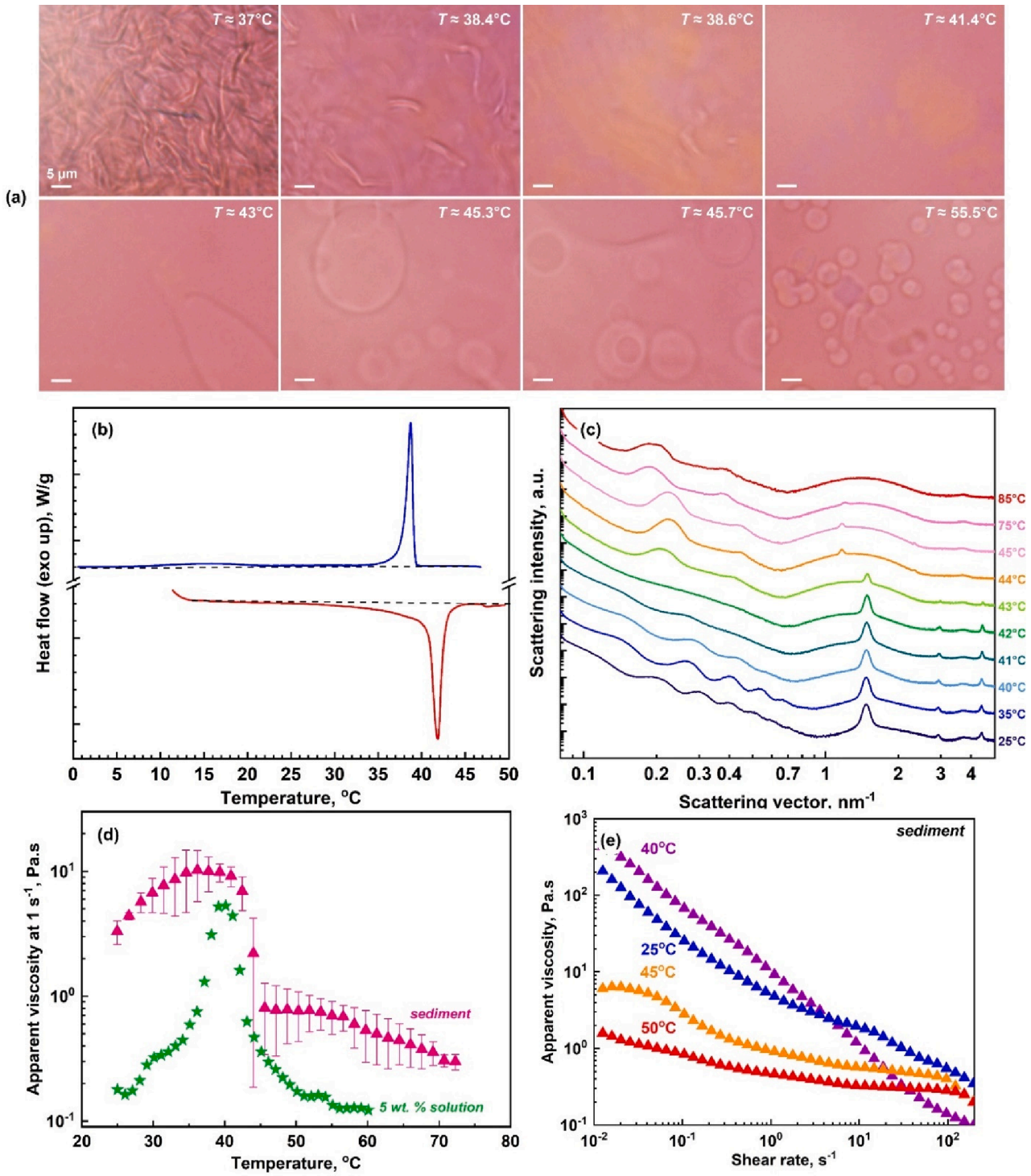

Fig. 6. Phase behavior of sediment upon heating. (a) Optical microscopy images in polarized light acquired upon sample heating. Scale bars = 5 μm. (b) DSC thermogram upon heating (red curve) and cooling (blue curve). (c) SAXS spectra obtained at different temperatures. A complementary WAXS spectra is available in Supplementary Fig. S5b. (d) Apparent viscosity measured at 1 s^{-1} shear rate upon 1 °C/min heating for the sediment (pink triangles) and for the 5 wt% solution before centrifugation (green stars). (e) Apparent viscosity of the sediment measured as a function of the applied shear rate. Data obtained at four different constant temperatures: 25 °C – blue symbols; 40 °C – purple; 45 °C – orange; 50 °C – red. (For interpretation of the references to color in this figure legend, the reader is referred to the web version of this article.)

5 wt% C_{16}SE solution contained ca. 16 wt% surfactant (as calculated from the DSC enthalpies and HPLC chromatograms). At this concentration, the molecular arrangement observed at 25 °C includes a network of partially fused diester particles covered by monoesters. Additionally, individual spherical diester particles are trapped within the network, along with some micelles primarily containing monoesters. The surfactant tails are in a solid state at this temperature.

The fluidization of the tails occurs at $T \approx 43$ °C. Slightly below this temperature, diester molecules begin to escape from the particles/network and arrange together with the monoesters, forming a lamellar phase and possibly a higher number of wormlike micelles occupying the whole solution volume. This leads to a significant viscosity increase.

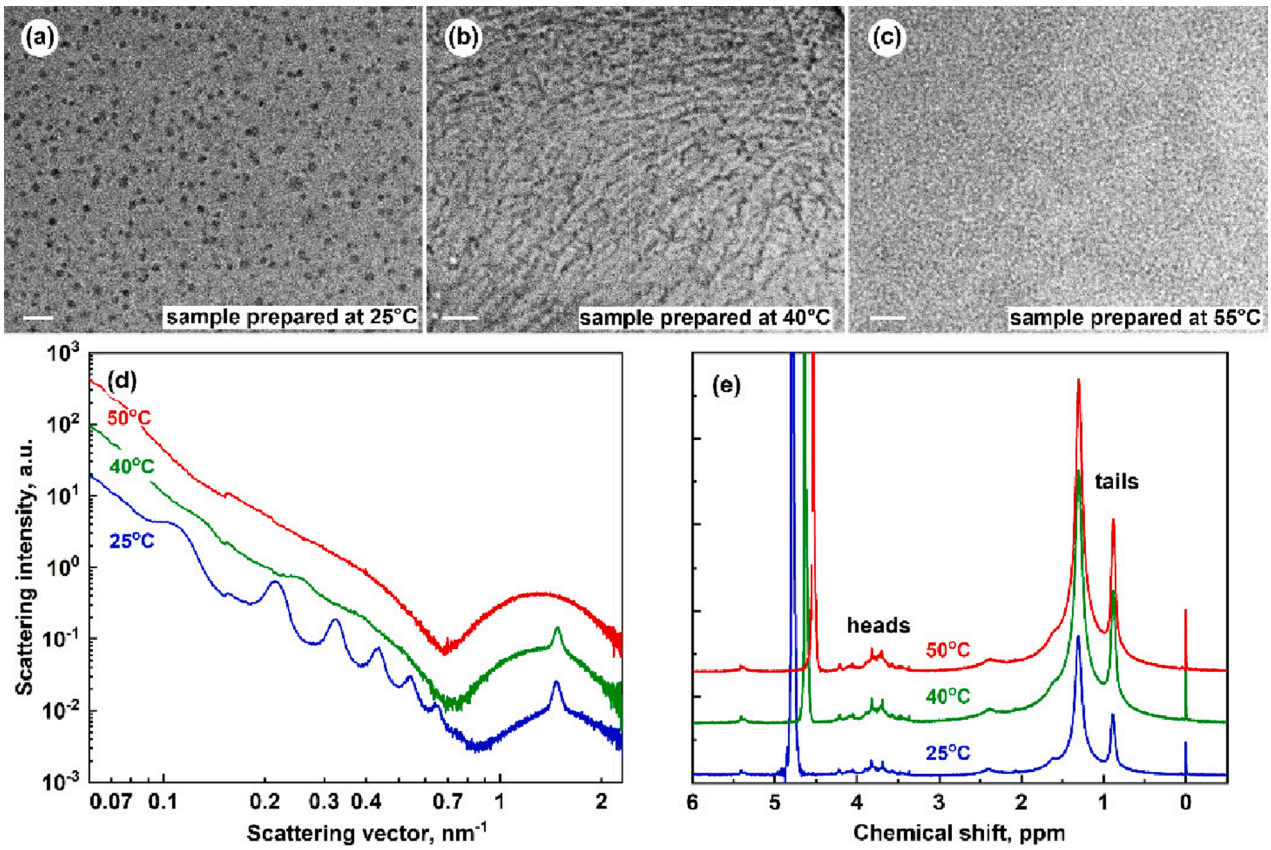

Fig. 7. (a-c) Cryo-TEM pictures of C_{16}SE solutions. The samples were prepared at: (a) 25 °C, (b) 40 °C and (c) 55 °C. Scale bars = 50 nm. (d) SAXS spectra obtained from 5 wt% C_{16}SE solution at different temperatures as denoted on the figure. (e) ^{1}H NMR of solution of 0.8 wt% C_{16}SE at 25 °C (blue curve), at 40 °C (red curve) and at 50 °C green curve. The spectra are shifted with respect to *y*-axis for clarity. (For interpretation of the references to color in this figure legend, the reader is referred to the web version of this article.)

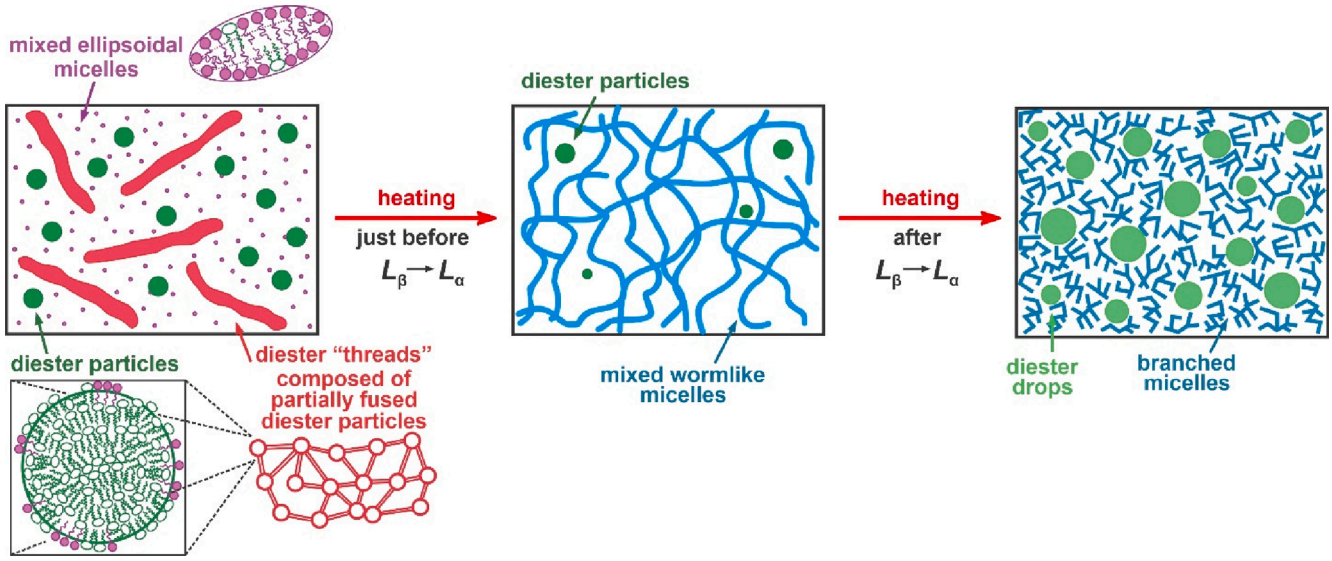

Fig. 8. Schematic representation of the molecular rearrangements proceeding in C_{16}SE solutions upon heating. The figure is not up to scale. See the text for more details.

Once the melting of the tails proceeds, the molecules become more mobile and cannot remain in the joint lamellar phase, leading to phase separation. The monoesters then form branched wormlike micelles with part of the diesters, while the excess diesters phase separates into distinct droplets.

A plausible explanation for the formation of relatively monodisperse nanodroplets observed in SAXS is that they are formed via a Plateau-Rayleigh type of capillary instability occurring in the partially fused network once the surfactant tails melt. This mechanism also explains the presence of uniform particles at low temperatures. We note that these

droplets were not observed in SAXS when the full C_{16}SE solution was studied, most probably because their concentration is too low to produce a scattering peak.

We also investigated whether the appearance of sediment at temperatures where the surfactant tails become fluid would change upon dilution with deionized water. This approach preserved the monoesters-to-diesters ratio while reducing the total surfactant concentration. The results showed that even when the surfactant concentration was decreased to 3–4 wt% to become comparable to the one found in the *top* phase, the diester droplets did not disappear, neither their faint colors, see Supplementary Figure S7. This result further confirms that the observed phase behavior is mainly determined by the monoesters-to-diesters ratio, rather than the total surfactant concentration, which, however, determines the absolute viscosities of the samples.

III. Monoesters: Diesters ≈ 4: 1

Finally, an intermediate case, where the monoesters prevail over diesters, yet their quantity is not sufficiently large to arrange all diesters in joint structures, is described. This occurs when commercially available surfactant is directly used to prepare surfactant solution. Here the monoesters to diesters ratio is ≈ 4:1, which is intermediate between the ratios found in the separated *serum* ≈ 7.5:1 (case I, above), and the 2.2:1 ratio seen in the centrifuged *sediment* (case II, above).

In agreement with these considerations, the behavior of full C_{16}SE solutions aligns closely with that observed in the sediments compared to the serum. This is schematically illustrated in Fig. 8 and can be explained as follows: At low temperature (25 °C), the main part of the diesters arrange into particles with diameter ca. 60 nm, some of which exist as individual particles in the solution while others form a partially fused network. These particles are stabilized by monoester molecules. However, the main part of monoesters arranges into slightly elongated ellipsoidal micelles. At elevated temperatures, the molecules gain energy and as the L_β-to-L_α phase transition temperature approaches, most diester molecules escape from the diester particles/network and arrange together with the monoester molecules into mixed wormlike micelles. A small part of diester particles remains in the sample, causing $\eta \propto \dot{\gamma}^{-0.9}$ instead of $\eta \propto \dot{\gamma}^{-1}$, as in the case of surfactant solutions, containing solely micellar network. Subsequently, once the L_β-to-L_α phase transition proceeds, diester molecules become more mobile and are excluded from this network, resulting in the formation of branched micellar network composed of monoesters and a small part of sucrose diester molecules. The main part of the diesters phase separate from the solution and form numerous droplets.

The described molecular rearrangement also explains the macroscopic rheological behavior observed in these systems. Specifically, the viscosity increase around $T \approx 40$ °C corresponds to the formation of mixed wormlike micelles between monoesters and diesters. Note that such micelles cannot be formed if the diesters fraction is significantly smaller. Furthermore, the subsequent viscosity decrease is attributed to another change in the micellar shape, due to the escape of diester molecules from the mixed micelles following the fluidization of their tails, leading to formation of branched micellar network whose rheological properties does not depend significantly on the surfactant concentration (for 1–5 wt% concentration range) and phase separation of the excess diester molecules into distinct droplets.

IV. Effect of monoesters-to-diesters ratio for the rheology of 2 wt% surfactant solutions

To quantify the effect of the monoesters to diesters ratio on the observed viscosity increase, additional experiments were conducted. The investigated samples were prepared by mixing specific quantities of serum and sediment, obtained from the initial 5 wt% C_{16}SE sample through centrifugation, in various ratios. These experiments were carried out at a fixed surfactant concentration of 2 wt%, achieved by adding the necessary amount of water to dilute the prepared solution. The mono- and diesters content in both the serum and sediment used for these experiments were determined using HPLC, see Supplementary Section S1.1 for detailed explanations of the experimental method. Moreover, HPLC and DSC analyses were performed on the obtained solutions to confirm their molecular composition (data not shown).

Fig. 9 illustrates the viscosity of the samples at 25 and 40 °C, as a function of the monoester content in the solution. The results unambiguously demonstrate that the increase in the monoesters content (respectively – the decrease in the amount of diesters) leads in an overall decrease in solution viscosity. As anticipated, the viscosity at 40 °C is notably higher than that observed at 25 °C. Additionally, the results directly demonstrate that the presence of only ca. 2 % diester molecules is already sufficient to induce slight viscosity increase upon heating. The effect becomes much more pronounced when the diester concentration is increased.

3.4.2. *Sucrose esters vs typical nonionic surfactants – Comparison of the observed rheological behavior*

In this section, we compare the currently observed rheological behavior with other examples for thermogelation previously shown in literature aiming to highlight the unique novel concepts described in this study for the first time.

Typically, solutions of water-soluble nonionic surfactants exhibit relatively low viscosities at concentrations up to ca. 15–20 wt% [49–52]. At this surfactant level, molecules arrange into spherical or slightly elongated micelles with relatively low volume fraction, incapable of inducing structuring throughout the entire solution volume.

In the present study, we demonstrate viscoelastic behavior in sucrose ester solutions, with zero-shear viscosity of ca. 1.3 Pa.s for 1 wt% C_{16}SE (Fig. 2d) and ca. 40 Pa.s for 5 wt% solution, see green stars in Fig. 10. Data for the viscosity of a typical nonionic surfactant, $C_{16}EO_{20}$ (Brij 58), at a 5 wt% concentration, is presented in Fig. 10 with the blue circles. As seen from the figure, this solution have much lower viscosity, η ≈ 0.018 Pa.s, which remains independent from the temperature throughout the studied range, between 25 and 65 °C. We note that at this surfactant concentrations, the micelles formed from $C_{16}EO_{20}$ molecules are only

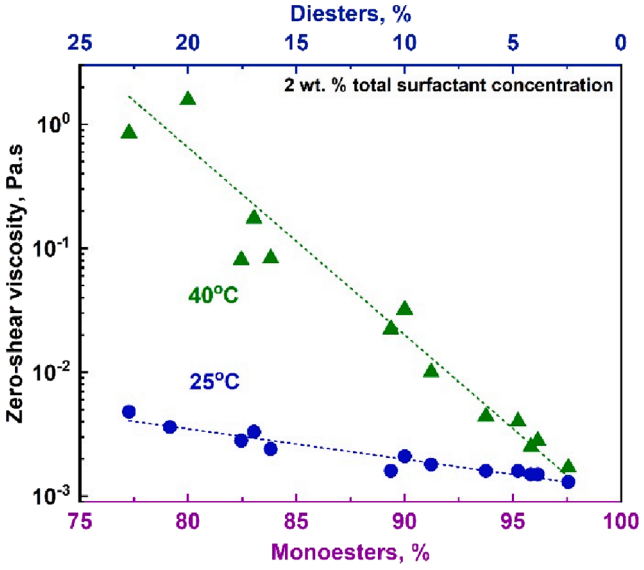

Fig. 9. Zero-shear viscosity for 2 wt% C_{16}SE solutions containing various monoesters-to-diesters ratios. The results are presented as a function of the percent monoesters calculated with respect to all surfactant molecules in the solution. Blue circles: 25 °C, green triangles: 40 °C. (For interpretation of the references to color in this figure legend, the reader is referred to the web version of this article.)

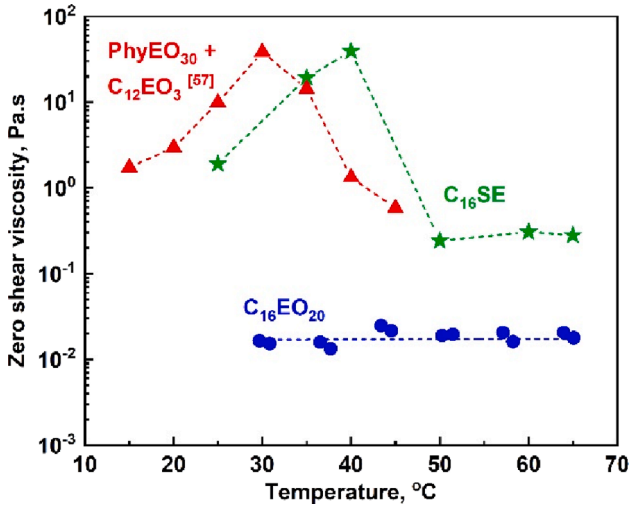

Fig. 10. Rheological behavior of aqueous nonionic surfactant solutions (total surfactant concentration = 5 wt%). Blue circles: behavior of typical nonionic surfactant, $C_{16}EO_{20}$. Green stars: data for $C_{16}SE$, obtained in the present study. Note that the viscosity remains constant after the maximum. Red triangles: data adapted from Ref. [57] showing the viscosity of solution containing 3.18 wt% polyoxyethylene (30) phytosterol and 1.82 wt% polyoxyethylene (3) dodecyl ether as function of the temperature. Note that the viscosity decreases continuously after the maximum. See the main text for more detailed explanations. (For interpretation of the references to color in this figure legend, the reader is referred to the web version of this article.)

slightly elongated ellipsoids.

As already explained, the viscosity increase observed in the $C_{16}SE$ solution with temperature variations is related to the disruption of the diester particles. These particles, initially separated as individual entities at lower temperatures, undergo (partial) rearrangement with the monoesters into entangled wormlike micelles which co-exist with a fraction of the diester particles remaining in the solution, see Fig. 8. To the best of our knowledge, this is the first study in which this specific mechanism for formation of wormlike micelles is revealed.

In our study, temperature was used as the primary trigger, therefore in the next lines we will focus on its effect for different surfactant systems. Generally, the increase of temperature results in an exponential decrease in the contour length of wormlike micelles, leading to an exponential decrease in the viscosity of the solutions [55,56]. In the $C_{16}SE$ solutions, however, the opposite trend was observed: viscosity increased until a maximum was reached, after which it gradually decreased but remained at a plateau value significantly higher than that typically observed for common ethoxylated nonionic surfactants, see Fig. 10.

Although not very common, viscoelastic behavior in wormlike micelles formed from nonionic surfactant solutions has been previously observed in several studies [51,55,57,58]. For example, Varade et al. [51] observed the formation of wormlike micelles in aqueous solutions of polysorbate 80 (polyoxyethylene sorbitan monooleate) and $C_{12}EO_3$ or $C_{14}EO_3$ (polyoxyethylene (3) dodecyl/tetradecyl ether) surfactants. Viscosity of ca. 0.04 Pa.s was demonstrated for a system containing 15 wt% polysorbate 80 and 3.07 wt% $C_{14}EO_3$ at 20 °C, which increased to ca. 2 Pa.s at 25 °C and to around 10 Pa.s at 30 °C [51]. Note that although the surfactant concentration is more than 3 times higher than that used in the present study, the highest viscosity demonstrated for this particular composition remains more than 3 times lower. The observed temperature-dependent thickening of polysorbate 80 and $C_{14}EO_3$ solutions was explained with enhanced one-dimensional growth of the wormlike micelles in the studied temperature range, as the temperature increase led to dehydration of polyoxyethylene chains, decreasing the molecular cross-sectional area and spontaneous curvature, while increasing the end cap energy [51].

In another study, Sharma et al. [57] demonstrated a significant viscosity increase in aqueous solutions of nonionic polyoxyethylene phytosterol surfactant ($PhyEO_{30}$) combined with $C_{12}EO_3$ surfactant at 5 wt% total surfactant concentration, see the red triangles in Fig. 10. Once again, the authors explained this behavior with the progressive dehydration of the ethoxy chains, promoting the one-dimensional growth over the formation of hemispherical end caps. The subsequent viscosity decay observed above 30 °C was attributed to increased micellar scission kinetics, leading to the formation of branched micelles [57]. Similarly, in another study by the same group, analogous results were demonstrated for 10 wt% $PhyEO_{30}$ surfactant combination with the oil-soluble monoglycerides – monopalmitin and monolaurin [58].

Several other studies have reached similar conclusions, see the comprehensive review in Ref. [55]. In all these studies, the increase of the viscosity in surfactant solutions containing nonionic wormlike micelles has been attributed to the favored micellar growth upon heating, facilitated by the dehydration of the ethoxy units up to a certain temperature. Furthermore, these investigations typically involved surfactant combinations with different hydrophilic heads (e.g., a combination of short and long polyoxyethylene blocks [57]) and/or different hydrophobic tails (e.g. oleic and lauric [51]). In contrast, our study demonstrates a conceptually distinct mechanism for viscosity increase, involving solely molecules with identical hydrophilic heads (sucrose) which does not contain ethoxy units, and which differ only in the number of hydrophobic tails (one or two) attached to the hydrophilic part of the surfactant molecule. Furthermore, the observed viscosity increase upon heating is not related to the dehydration of the ethoxy units, but rather to the reorganization of the diester molecules occurring at temperature close to their phase transition temperature.

3.4.3. *Examples for other systems undergoing thermogelation*

Wormlike micelles are typically formed in solutions of ionic surfactants in various cases [53,54], including in solutions where both anionic and cationic surfactants are included; when ionic surfactant is combined with zwitterionic surfactant; or when suitable electrolytes are introduced. In most cases, the formation of wormlike micelles become possible only when the electrostatic repulsion between the charged headgroups is appropriately screened. A comprehensive review about the wormlike micelles which can react to various triggers, including pH and temperature variations, light, CO_2, redox reactions, and other external factors in available in Ref. [55].

Thermo-thickening behavior has been also observed in several ionic surfactant systems, usually in the presence of strong hydrotropes [59–63]. For example, in a study involving the C_{22}-tailed cationin surfactant containing a double bond between C9 and C10 atoms, erucyl bis-(hydroxyethyl)methylammonium chloride (EHAC) with the aromatic salt sodium hydroxynaphtalene carboxylate (SHNC), wormlike micelles formed upon heating and led to viscosity increase [60]. This viscosity increase was attributed to changes in the solubility of the HNC^- anions. At low temperatures, the hydrophobic anions have low solubility in water and bind strongly to the positively charged surfactant micelles, even rendering them negatively charged. As the temperature rises, the solubility of the anions increases, causing their desorption, thus reducing the micellar surface charge and enabling the growth of wormlike micelles. This phenomenon occurs only when the SHNC concentration is not too high, because in this case the change in the solubility will have an insignificant effect over the micelle charge, and also for salt which is relatively hydrophobic and able to attach to surfactant micelles, no such effect is observed if NaCl of KCl are added to the EHAC solution [60]. Similar mechanisms for increase of the solutions viscosity upon heating are reported in Refs [55,59,61–63], where different ionic surfactants are combined with hydrophobic salts, which change their solubility upon temperature changes, thus allowing change of the interfacial curvature and transition into wormlike micelles. These mechanisms are distinctively different from the one described in the

present study.

Notably, in many cases the viscosity peak is observed within the 40–60 °C temperature range. Although this appear to be a common phenomenon, the underlying mechanisms vary, incl. change in the salt/surfactant solubility, melting of the surfactant tails, and dehydration of the ethoxy groups upon heating. The surfactants studied typically feature C16 or C18 hydrophobic tails, which are expected to undergo phase transition within this temperature range. Therefore, further investigation about the effect of surfactant tails on the observed thermothickening phenomenon is needed to determine whether and how the changes in tail ordering contribute to these processes.

4. Conclusions

The current study explores the supramolecular structures formed in aqueous solutions of the nonionic sucrose palmitate surfactant at different temperatures and at various monoesters to diesters ratios. We show that diluted solutions (1–5 wt%) of the commercial C_{16}SE surfactant possess viscoelastic properties and their viscosity passes through a maximum at temperature around 40 °C. Similar behavior have been observed previously for sucrose stearate surfactant [25–27]. However, although it has been attributed to the formation of wormlike micelles, the intricate molecular processes driving this phenomenon have not been revealed so far.

The results from the presently performed experiments reveal the mechanisms governing the observed phenomena. These mechanisms are related to the co-existence of monoester and diester molecules in the studied surfactant. The diester molecules undergo phase transition upon heating. At temperatures below the phase transition temperature, diester molecules are organized either in diester particles or in a network of partially fused particles and do not contribute significantly to the solution viscosity in studied concentration range (between 1 and 5 wt %). At these temperatures, the monoester molecules form slightly elongated micelles which do not increase significantly the viscosity. Around the phase transition temperature, the diester molecules escape from the particles and start to incorporate in the monoester micelles. This leads to increase of the packing parameter which ensures formation of long wormlike micelles. As a consequence, the viscosity of the solutions increases more than 10^3-fold. Further increase of temperature leads to the melting of all diester molecules which incorporate in the micelles, thus changing once again their packing parameter. At that stage the formation of branched micelles is facilitated and part of diester molecules become separated as individual drops. This results in a decrease of the observed viscosity, but it remains higher than that observed at low temperatures. Furthermore, it becomes almost concentration independent in the 1–5 wt% concentration range due to the formation of saturated branched micelles. The observed changes in phase behavior are related to changes in the arrangement of the hydrocarbon surfactant tails. At lower temperatures, the tails are in a frozen state (gel phase), while the temperature increase induces their fluidization, governing the observed processes.

Our investigation of solutions with varying compositions of monoesters and diesters reveals that the observed viscosity increase at a constant surfactant concentration correlates with the fraction of diesters present. Even with just ca. 2 % diester molecules (calculated relative to all surfactant molecules in the solution), a slight viscosity increase is evident upon heating. As the concentration of diesters increases, this effect becomes significantly more pronounced.

We note that the mechanism described for viscosity increase and the formation of wormlike micelles in nonionic systems has not been described previously and it is distinctly different from the typical behavior observed upon heating of nonionic surfactant solutions. Typically, much higher surfactant concentrations are required to induce the formation of wormlike micelles [55]. Furthermore, upon heating, the viscosity of wormlike micelles typically decreases due to enhanced scissoring kinetics and a decrease in their contour length [55]. Somewhat similar rheological behavior to that demonstrated for sucrose esters, has been observed in certain special ethoxylated nonionic surfactant mixtures [51,55,57,58] and in some ionic systems [55,59–63]. However, this behavior has been attributed to the dehydration of the polyoxyethylene units upon heating, leading to preferential one-dimensional growth due to increased end cap energy for the nonionic surfactants [51]. In the ionic systems, the thermogelation has been observed in presence of strong hydrotropes, which changed their solubility upon temperature variations [59–61]. These mechanisms are distinctly different from the one revealed in the present study.

This study represents a significant advancement in understanding the phase behavior of the biodegradable sucrose ester surfactants, which are widely used in diverse industrial applications. It is expected to serve as a foundational point for future research into the phase behavior of other sucrose-based surfactants and for surfactants composed of mixtures of molecules undergoing temperature-induced changes in their physical state. Additionally, this study will facilitate in elucidating the impact of various factors on the observed behavior with sucrose esters, such as ionic strength, the addition of proteins or particles, the mixing of different surfactants, and more.

CRediT authorship contribution statement

N. Pagureva: Investigation, Formal analysis, Writing – original draft. **D. Cholakova:** Writing – review & editing, Writing – original draft, Validation, Methodology, Investigation, Formal analysis, Conceptualization. **Z. Mitrinova:** Investigation, Formal analysis. **M. Hristova:** Investigation. **N. Burdzhiev:** Investigation. **S. Tcholakova:** Writing – review & editing, Writing – original draft, Validation, Methodology, Investigation, Formal analysis, Conceptualization.

Declaration of competing interest

The authors declare that they have no known competing financial interests or personal relationships that could have appeared to influence the work reported in this paper.

Data availability

Data will be made available on request.

Acknowledgements

This study was funded by the European Union-Next GenerationEU, through the National Recovery and Resilience Plan of the Republic of Bulgaria, project No BG-RRP-2.004-0008. The authors are grateful to Mrs. K. Rusanova and Assoc. Prof. L. Mihaylov (Sofia University) for cryo-TEM imaging. The authors thank P. Borisov, M. Pantov and H. Bletsova (Sofia University) for performing some fraction of the experiments. The valuable help of V. Petkov and V. Georgiev (Sofia University) with the chemical analysis is greatly appreciated. The authors acknowledge the possibility to use SAXS/WAXS instrument purchased for execution of project BG05M2OP001-1.002-0012, Operational Program “Science and Education for Smart Growth”, Bulgaria.

Appendix A. Supplementary material

Supplementary data to this article can be found online at https://doi.org/10.1016/j.jcis.2024.06.061.

References

[1] M. Lukic, I. Pantelic, S. Savic, An overview of novel surfactants for formulation of cosmetics with certain emphasis on acidic active substances, Tenside Surf, Det. 53 (2016) 7–19, https://doi.org/10.3139/113.110405.

[2] S. Stubbs, S. Yousaf, I. Khan, A review on the synthesis of bio-based surfactants using green chemistry principles, J. Pharm. Sci. 30 (2022) 407–426, https://doi.org/10.1007/s40199-022-00450-y.

[3] K. Chansanroj, G. Betz, Sucrose esters with various hydrophilic-lipophilic properties: novel controlled release agents for oral drug delivery matrix tablets prepared by direct compaction, Acta Biomater 6 (2010) 3101–3109, https://doi.org/10.1016/j.actbio.2010.01.044.

[4] I. Trabelsi, K. Essid, M.H. Frikha, Synthesis of sucrose fatty acid esters by using mixed carboxylic-fatty anhydrides, J. Oleo Sci. 69 (2020) 693–701, https://doi.org/10.5650/jos.ess19239.

[5] Y. Teng, S. Stewart, Y.-W. Hai, X. Li, M. Banwell, P. Lan, Sucrose fatty acid esters: synthesis, emulsifying capacities, biological activities and structure-property profiles, Crit. Rev. Food Sci. Nutr. 61 (2021) 3297-3317, doi; 10.1080/10408398.2020.1798346.

[6] I. Baker, B. Matthews, H. Suares, I. Krodkiewska, D. Neil Furlong, F. Grieser, C. Drummond, Sugar fatty acid ester surfactants: Structure and ultimate aerobic biodegradability, J. Surf. Deterg. 3 (2000) 1–11, https://doi.org/10.1007/s11743-000-0107-2.

[7] I. Baker, R. Ian Willing, D. Neil Furlong, F. Grieser, C. Drummond, Sugar fatty acid ester surfactants: Biodegradation pathways, J. Surf. Deterg. 3 (2000) 13–27, https://doi.org/10.1007/s11743-000-0108-1.

[8] J. Vargas, J. Ortega, G. Metzker, J. Larrahondo, M. Boscolo, Natural sucrose esters: Perspectives on the chemical and physiological use of an under investigated chemical class of compounds, Phytochem. 177 (2020) 112433, doi; 10.1016/j.phytochem.2020.112433.

[9] M. Nakayama, D. Tomiyama, K. Ikeda, M. Katsuki, A. Nonaka, T. Miyamoto, Antibacterial effects of monoglycerol fatty acid esters and sucrose fatty acid esters on bacillus spp, Food Sci, Techn. Res. 21 (2015) 431–437, https://doi.org/10.3136/fstr.21.431.

[10] M. Habulin, S. Sabeder, Z. Knez, Enzymatic synthesis of sugar fatty acid esters in organic solvent and in supercritical carbon dioxide and their antimicrobial activity, J. Supercritical Fluids 45 (2008) 338–345, https://doi.org/10.1016/j.supflu.2008.01.

[11] W. Snoch, D. Wnuk, T. Witko, J. Staroń, A. Bojarski, E. Jarek, F. Plou, M. Guzik, In Search of Effective Anticancer Agents—Novel Sugar Esters Based on Polyhydroxyalkanoate Monomers, Int. J. Mol. Sci. 22 (2021) 7238, doi; 10.3390/ijms22137238.

[12] C. Walker, Food applications of sucrose esters, Cereal Foods World 29 (1984) 286–289.

[13] M. Younes, P. Aggett, F. Aguilar, R. Crebelli, B. Dusemund, M. Filipič, M. Frutos, P. Galtier, D. Gott, U. Gundert-Remy, G. Kuhnle, C. Lambré, I. Lillegaard, P. Moldeus, A. Mortensen, A. Oskarsson, I. Stankovic, I. Waalkens-Berendsen, R. Woutersen, M. Wright, P. Boon, O. Lindtner, C. Tlustos, A. Tard, J.-C. Leblanc, Refined exposure assessment of sucrose esters of fatty acids (E 473) from its use as a food additive, EFSA J. 16 (2018) e05087, doi; 10.2903/j.efsa.2018.5087.

[14] F. Aguilar, U. Charrondiere, B. Dusemund, P. Galtier, J. Gilbert, D. Gott, S. Grilli, R. Guertler, J. Koenig, C. Lambré, J.-C. Larsen, J.-C. Leblanc, A. Mortensen, D. Parent-Massin, I. Pratt, I. Rietjens, I. Stankovic, P. Tobback, T. Verguieva, R. Woutersen, Scientific Opinion on the safety of sucrose esters of fatty acids prepared from vinyl esters of fatty acids and on the extension of use of sucrose esters of fatty acids in flavourings, EFSA J. 8 (2010) 1512, https://doi.org/10.2903/j.efsa.2010.1512.

[15] A. Szűts, P. Szabó-Révész, Sucrose esters as natural surfactants in drug delivery systems - A mini-review, Int. J. Pharm. 433 (2012) 1–9, https://doi.org/10.1016/j.ijpharm.2012.04.076.

[16] D. Zhi, J. Shi, S. Cui, T. Yang, J. Yang, W. Wang, P. Ma, Y. Zhen, S. Zhang, Biodegradable sucrose ester-based cationic lipids as novel vectors for efficient and safe delivery of IGF-1R siRNA, ACS Mater. Lett. 5 (2023) 862–873, https://doi.org/10.1021/acsmaterialslett.2c00994.

[17] T. Polat, R. Linhardt, Syntheses and applications of sucrose-based esters, J. Surf. Deterg. 4 (2001) 8415–8421, https://doi.org/10.1007/s11743-001-0196-y.

[18] Y.-G. Shi, J.-R. Li, Y.-H. Chu, Enzyme-catalyzed regioselective synthesis of sucrose-based esters, J. Chem. Techn. Biotechn. 86 (2011) 1457–1468, https://doi.org/10.1002/jctb.2711.

[19] T. Herrington, S. Sahi, Phase behavior of some sucrose surfactants with water and n-decane, J. Am. Oil Chem. Soc. 65 (1988) 1677–1681, https://doi.org/10.1007/BF02912575.

[20] T. Sato, D. Acharya, M. Kaneko, K. Aramaki, Y. Singh, M. Ishitobi, H. KuniedaSato, Oil-induced structural change of wormlike micelles in sugar surfactant systems, J. Disper. Sci. Techn. 27 (2006) 611–616, https://doi.org/10.1080/01932690600660632.

[21] M. Yamamoto, H. Ando, S. Arima, K. Aramaki, Rheological properties of wormlike micelles solutions being available in wide temperature range in sucrose palmitate systems, J. Oleo Sci. 58 (2009) 303–311, https://doi.org/10.5650/jos.58.303.

[22] A. Szűts, M. Budai-Szűcs, I. Erős, N. Otomo, P. Szabó-Révész, Study of gel-forming properties of sucrose esters for thermosensitive drug delivery systems, Int. J. Pharm. 383 (2010) 132–137, https://doi.org/10.1016/j.ijpharm.2009.09.013.

[23] K. Aramaki, S. Hoshida, S. Arima, Effect of carbon chain length of cosurfactant on the rheological properties of nonionic wormlike micellar solutions formed by a sugar surfactant and monohydroxy alcohols, Colloids Surf, A: Physicochem. Eng. Aspects 366 (2010) 58–62, https://doi.org/10.1016/j.colsurfa.2010.05.011.

[24] K. Aramaki, S. Hoshida, S. Arima, Formation of wormlike micelles with natural-sourced ingredients (sucrose fatty acid ester and fatty acid) and a viscosity-boosting effect induced by fatty acid soap, Colloids Surf, A: Physicochem. Eng. Aspects 396 (2012) 278–282, https://doi.org/10.1016/j.colsurfa.2012.01.009.

[25] C. Calahorro, J. Muñoz, M. Berjano, A. Guerrero, C. Gallegos, Flow behavior of sucrose stearate/water systems, J. Am. Oil Chem. Soc. 69 (1992) 660–666, https://doi.org/10.1007/BF02635806.

[26] V. Sadtler, M. Guely, P. Marchal, L. Choplin, Shear-induced phase transitions in sucrose ester surfactant, J. Colloid Interface Sci. 270 (2004) 270–275, https://doi.org/10.1016/j.jcis.2003.10.038.

[27] S. Takahashi, I. Kaneda, A transient network structure in sucrose stearate/water systems, Nihon Reoroji Gakkaishi, J. Soc. Rheology, Japan 42 (2014) 103–109, https://doi.org/10.1678/rheology.42.103.

[28] P. Carreau, D. De Kee, M. Daroux, An analysis of the viscous behaviour of polymeric solutions, Can. J. Chem. Eng. 57 (1979) 135–140, https://doi.org/10.1002/cjce.5450570202.

[29] S.E. Anachkov, G.S. Georgieva, L. Abezgauz, D. Danino, P.A. Kralchevsky, Viscosity peak due to shape transition from wormlike to disklike micelles: Effect of dodecanoic acid, Langmuir 34 (2018) 4897–4907, https://doi.org/10.1021/acs.langmuir.8b00421.

[30] Y. Ishigami, H. Machida, Vesicles from sucrose fatty acid esters, J. Am. Oil Chem. Soc. 66 (1989) 599–603, https://doi.org/10.1007/BF02885457.

[31] R. Zheng, X. Hu, C. Su, J. Jiang, Z. Cui, B. Binks, Edible oil-water foamulsions stabilized by vesicle network of sucrose ester, J. Molecular Liquids 371 (2023) 121066, doi; 10.1016/j.molliq.2022.121066.

[32] X. Hu, B. Binks, Z. Cui, High internal phase emulsions stabilized by adsorbed sucrose stearate molecules and dispersed vesicles, Food Hydrocolloids 121 (2021) 107002, doi; 10.1016/j.foodhyd.2021.107002.

[33] R. Nagarajan, Molecular packing parameter and surfactant self-assembly: The neglected role of the surfactant tail, Langmuir 18 (2002) 31–38, https://doi.org/10.1021/la010831y.

[34] V. Katev, Z. Vinarov, S. Tcholakova, Mechanisms of drug solubilization by polar lipids in biorelevant media, Eur. J. Pharm. Sci. 159 (2021) 105733, doi; 10.1016/j.ejps.2021.105733.

[35] S. Tsibranska-Gyoreva, V. Petkov, V. Katev, D. Krastev, Z. Vinarov, S. Tcholakova, Cholesterol solubilization: Interplay between phytosterols, saponins and lipid digestion products, Colloids and Surfaces A: Physicochem. Eng. Aspects 662 (2023) 131052, doi; 10.1016/j.colsurfa.2023.131052.

[36] D. Cholakova, N. Denkov, S. Tcholakova, I. Lesov, S. Smoukov, Control of drop shape transformations in cooled emulsions, Adv. Colloid Interface Sci. 235 (2016) 90–107, https://doi.org/10.1016/j.cis.2016.06.002.

[37] D. Cholakova, N. Denkov, S. Tcholakova, Zh. Valkova, S. Smoukov, Multilayer formation in self-shaping emulsion droplets, Langmuir 35 (2019) 5484–5495, https://doi.org/10.1021/acs.langmuir.8b02771.

[38] N.A. Spenley, M.E. Cates, T.C.B. McLeish, Nonlinear rheology of wormlike micelles, Phys. Rev. Lett. 71 (1993) 939–942, https://doi.org/10.1103/PhysRevLett.71.939.

[39] Z. Mitrinova, S. Tcholakova, J. Popova, N. Denkov, B. Dasgupta, K. P. Ananthapadmanabhan, Efficient control of the rheological and surface properties of surfactant solutions containing C8–C18 fatty acids as cosurfactants, Langmuir 29 (2013) 8255–8265, https://doi.org/10.1021/la401291a.

[40] Y.-Y. Won, A. Brannan, H. Ted Davis, F.S. Bates, Cryogenic transmission electron microscopy (Cryo-TEM) of micelles and vesicles formed in water by poly(ethylene oxide)-based block copolymers, J. Phys Chem B 106 (2002) 3354–3364, https://doi.org/10.1021/jp013639d.

[41] D. Danino, Cryo-TEM of soft molecular assemblies, Curr. Opin. Colloid Interface Sci. 17 (2012) 316–329, https://doi.org/10.1016/j.cocis.2012.10.003.

[42] D. Cholakova, D. Glushkova, M. Pantov, S. Tcholakova, N. Denkov, Triglyceride mixtures: Cold-bursting and double emulsion formation, Colloids Surf. A 668 (2023) 131439, https://doi.org/10.1016/j.colsurfa.2023.131439.

[43] N. Raval, R. Maheshwari, D. Kalyane, S. R. Youngren-Ortiz, M. B. Chougule, R. K. Tekade, Chapter 10: Importance of physicochemical characterization of nanoparticles in pharmaceutical product development in *Basic fundamentals of drug delivery* (2019) 369-400. doi; 10.1016/B978-0-12-817909-3.00010-8.

[44] T. Narayanan, Chapter 17: Synchrotron small-angle X-ray scattering in *Soft-matter characterization* Springer-Verlag Berlin Heidelberg (2008) 900-952. doi; 10.1007/978-1-4020-4465-6_17.

[45] R.J. Roe, Methods of X-ray and neutron scattering in polymer science, Oxford University Press, 2000.

[46] M. Kanemaru, S. Kuwahara, K. Yamamoto, Y. Kaneko, J. Kadokawa, Self-assembly of 6-*O*- and 6'-*O*-hexadecylsucroses mixtures under aqueous conditions, Carbohydr. Res. 345 (2010) 2718–2722, https://doi.org/10.1016/j.carres.2010.10.003.

[47] M. Kranenburg, B. Smit, Phase behavior of model lipid bilayers, J. Phys. Chem. 109 (2005) 6553–6563, https://doi.org/10.1021/jp0457646.

[48] M.L. Manca, I. Castangia, P. Matricardi, S. Lampis, X. Fernandez-Busquets, A. M. Fadda, M. Manconi, Molecular arrangements and interconnected bilayer formation induced by alcohol or polyalcohol in phospholipid vesicles, Colloids Surf. B: Biointerfaces 117 (2014) 360–367, https://doi.org/10.1016/j.colsurb.2014.03.010.

[49] A. Heins, V.M. Garamus, B. Steffen, H. Stockmann, K. Schwarz, Impact of phenolic antioxidants on structural properties of micellar solutions, Food Biophys. 1 (2006) 189–201, https://doi.org/10.1007/s11483-006-9020-5.

[50] Y. Shimada, Y. Kawabata, T. Kato, Rheological properties of wormlike micelles formed in concentrated region of nonionic surfactant ($C_{16}E_7$) – water system, Colloid Polym. Sci. 293 (2015) 3275-3283. doi; s00396-015-3776-4.

[51] D. Varade, K. Ushiyama, L. K. Shrestha, K. Aramaki, Wormlike micelles in Tween 80/C_mEO_3 mixed nonionic surfactant systems in aqueous media, J. Colloid Interface Sci. 312 (2007) 489-497. doi; j.jcis.2007.02.090.

[52] S.C. Sharma, K. Tsuchiya, K. Sakai, H. Sakai, M. Abe, Viscoelastic wormlike micellar solutions in mixed environmentally friendly nonionic surfactant systems, Colloids Surf A 335 (2009) 23–27, https://doi.org/10.1016/j.colsurfa.2008.10.022.
[53] J. Yang, Viscoelastic wormlike micelles and their applications, Current Opin. Colloid Interface Sci. 7 (2002) 276–281, https://doi.org/10.1016/S1359-0294(02)00071-7.
[54] D. Acharya, H. Kunieda, Wormlike micelles in mixed surfactant solutions, Adv. Colloid Interface Sci. 123–126 (2006) 401–413, https://doi.org/10.1016/j.cis.2006.05.024.
[55] Z. Chu, C.A. Dreiss, Y. Feng, Smart wormlike micelles, Chem. Rev. Soc. 42 (2013) 7174–7203, https://doi.org/10.1039/C3CS35490C.
[56] S.J. Candau, E. Hirsch, R. Zana, M. Delsanti, Rheological properties of semidilute and concentrated aqueous solutions of cetyltrimetylammonium bromide in the presence of potassium bromide, Langmuir 5 (1989) 1225–1229, https://doi.org/10.1021/la00089a018.
[57] S.C. Sharma, L.K. Shrestha, K. Tsuchiya, K. Sakai, H. Sakai, M. Abe, Viscoelastic wormlike micelles of long polyoxyethylene chain phytosterol with lipophilic nonionic surfactant in aqueous solution, J. Phys. Chem. B 113 (2009) 3043–3050, https://doi.org/10.1021/jp8102244.
[58] S.C. Sharma, L.K. Shrestha, K. Sakai, H. Sakai, M. Abe, Viscoelastic solution of long polyoxyethylene chain phytosterol/monoglyceride/water systems, Colloid Polym. Sci. 288 (2010) 405–414, https://doi.org/10.1007/s00396-009-2135-8.
[59] Y. Feng, Z. Chu, C.A. Dreiss, *Smart wormlike micelles. Design, characteristics and applications*, Chapter 2: Thermo-responsive wormlike micelles, Springer, Berlin, Heidelberg, 2015, pp. 7–27.
[60] G.C. Kalur, B.D. Frounfelker, B.H. Cipriano, A.I. Norman, S.R. Raghavan, Viscosity increase with temperature in cationic surfactant solutions due to the growth of wormlike micelles, Langmuir 21 (2005) 10998–11004, https://doi.org/10.1021/la052069w.
[61] T.S. Davies, A.M. Ketner, S.R. Raghavan, Self-assembly of surfactant vesicles that transform into viscoelastic wormlike micelles upon heating, J. Am. Chem. Soc. 128 (2006) 6669–6675, https://doi.org/10.1021/ja060021e.
[62] Z. Chu, Y. Feng, Thermo-switchable surfactant gel, Chem. Commun. 47 (2011) 7191–7193, https://doi.org/10.1039/c1cc11428j.
[63] Q. Yin, Q. Tian, J. Doutch, A.O. Frimpong, X. Xu, H. Yin, P. Li, Y. Feng, An insight into the thermo-thickening behavior of wormlike micellar solutions based on ultra-long-chain surfactants, Phys. Chem. Chem. Phys. 24 (2022) 11112–11123, https://doi.org/10.1039/D2CP00687A.